THE JOURNAL OF PHYSICAL CHEMISTRY B

Article

pubs.acs.org/JPCB

Ultra-Broadband Dielectric and Optical Kerr-Effect Study of the Ionic Liquids Ethyl and Propylammonium Nitrate

Thomas Sonnleitner,[†] David A. Turton,[‡] Glenn Hefter,[§] Alexander Ortner,[∥] Stefan Waselikowski,[∥] Markus Walther,[∥] Klaas Wynne,[‡] and Richard Buchner*[,†]

[†]Institut für Physikalische und Theoretische Chemie, Universität Regensburg, Universitatsstr. 31, D-93040 Regensburg, Germany

[‡]School of Chemistry, University of Glasgow, University Avenue, Glasgow G12 8QQ, United Kingdom

[§]Chemistry Department, Murdoch University, Murdoch, W.A. 6150, Australia

[∥]Department of Molecular and Optical Physics, Albert-Ludwigs-Universität Freiburg, Hermann-Herder-Str. 3, 79104 Freiburg, Germany

Supporting Information

ABSTRACT: Dielectric relaxation (DR) and optical Kerr-effect (OKE) spectra of the archetypal protic ionic liquids ethyl- and propylammonium nitrate (EAN and PAN) have been measured over an unusually large frequency range from 200 MHz to 10 THz at temperatures (mostly) between 5 and 65 °C. Analysis of the low-frequency α-relaxation, associated with the cooperative relaxations of the cations (DR) and anions (OKE) and any clusters present, indicated that ion reorientation in EAN is decoupled from viscosity and occurs via cooperative relaxation involving large-angle jumps rather than rotational diffusion. Detailed consideration of the high-frequency parts of the DR and OKE spectra showed that the observed intensities were a complex combination of overlapping and possibly coupled modes. In addition to previously identified intermolecular H-bond vibrations, there are significant contributions from the librations of the cations and anions. The present assignments were shown to be consistent with the isotopic shifts observed for deuterated EAN.

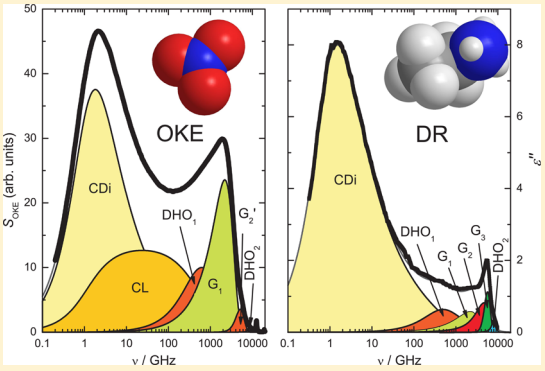

1. INTRODUCTION

Protic ionic liquids (PILs) are a subgroup of room-temperature ILs that are produced via proton transfer by combining a Brønsted acid with a Brønsted base.[1] The presence of proton-donor and proton-acceptor sites is the key characteristic of PILs that distinguishes them from aprotic ILs and explains their ability to form extended hydrogen-bond networks among their cations and anions.[2] Depending on the degree of proton transfer from acid to base, PILs usually have a non-negligible vapor pressure, and some of them can be distilled at reduced pressure,[3] having boiling points below their decomposition temperatures.[4] PILs have attracted particular interest as possible replacements for aqueous electrolyte solutions in batteries and fuel cells, where their relatively high electrical conductivity, via ion or proton conduction, is of major importance.[5,6] However, to tap the full potential of PILs for industrial and scientific applications, detailed knowledge of their liquid structure and their microscopic dynamics is essential.

Undoubtedly the best known PIL is ethylammonium nitrate (EAN, $[EtNH_3^+][NO_3^-]$), which was first investigated almost 100 years ago by Walden.[7] This salt has received considerable attention over the past few years as a model PIL due to its relatively straightforward chemical structure and also as a possible analogue for water.[1,2,8] Recent studies of this important compound have included small-angle neutron scattering (SANS),[9] X-ray diffraction (XRD),[10] and molecular dynamics (MD) simulations.[11,12] Of more immediate relevance to the present investigation, Fumino et al.[13,14] have reported the far-infrared (FIR) spectra of EAN and related compounds, while Weingärtner and coworkers[15] have measured the dielectric spectrum of EAN up to 40 GHz over the temperature range, $15 \leq \vartheta/°C \leq 80$, subsequently extending their 25 °C spectrum to 2 THz using time-domain terahertz spectroscopy (THz-TDS).[16]

The latter studies[15,16] have established some important properties of EAN including its static permittivity or dielectric constant, ε_s. The presence of low-energy modes in the FIR spectrum of EAN and related compounds has attracted special interest[13] because of their apparent similarity to some of the H-bond modes in water. However, unambiguous interpretation of these weak modes is not easy, particularly when using information from only one technique. For this reason, Fumino et al.[13] employed density functional theory (DFT) calculations

Special Issue: Branka M. Ladanyi Festschrift

Received: March 25, 2014
Revised: June 16, 2014
Published: June 19, 2014

   dx.doi.org/10.1021/jp502935t | J. Phys. Chem. B 2015, 119, 8826−8841

to assist with their assignments. Nevertheless, a comprehensive understanding of the structure and dynamics of liquid EAN is still lacking.

The combination of ultrafast optical Kerr-effect (OKE) and broadband dielectric relaxation (DR) spectroscopies, especially when augmented by THz-TDS and FIR measurements, has been shown to be a powerful means of investigating the structure and dynamics of imidazolium-based aprotic ILs.[17−19] Accordingly, the present paper presents a detailed ultra-boadband study of EAN that utilizes all of these techniques. These measurements cover the exceptionally broad frequency range from ∼200 MHz to 10 THz at temperatures $5 \leq \vartheta/°C \leq 65$ and are supplemented by DR spectra of propylammonium nitrate (PAN) along with limited measurements on partially deuterated (d_3-)EAN at 25 °C. A preliminary discussion of some of these data has appeared[18] but is significantly extended here by additional DR measurements on EAN, PAN, and d_3-EAN, high-precision data for conductivity and viscosity, and a more detailed quantitative analysis of the OKE and DR spectra as a whole. In particular, a comprehensive examination of the important high-frequency processes is presented.

2. EXPERIMENTAL SECTION

2.1. Materials. Two batches of EAN were used. The first, which was synthesized according to Evans et al.,[20] was used for all DR, OKE, viscosity, and density measurements. For the conductivity measurements and deuteration, a commercial sample of EAN (>97%, Iolitec, Heilbronn, Germany) was employed. Both batches were dried under vacuum ($p < 10^{-8}$ bar) for 12 days at 40 °C to minimize their water content, yielding 95 ppm of H_2O by coulometric Karl Fischer titration for the first and 20 ppm of H_2O for the second batch. For the commercial sample, halide impurities were specified by the manufacturer to be <100 ppm. The purity of all samples was further confirmed by ^{1}H NMR spectroscopy, which showed no detectable ^{1}H-containing impurities.

Partially deuterated d_3-EAN was prepared by adding fresh D_2O (99.9%, Deutero, Kastellaun, Germany) to commercial EAN and stirring for 24 h. The solution was then evaporated under vacuum, and the whole process was repeated. The product so obtained was found to be 91% deuterated, corresponding to an average composition of $[EtND_{2.7}H_{0.3}]^+$; its water content was 145 ppm.

The PAN sample was provided by QUILL at Queen's University, Belfast, Ireland and was prepared by dropwise addition of concentrated nitric acid to a cold solution of propylamine. The product was dried by lyophilization for 24 h at $p = 0.4$ mbar to give a pale-yellow liquid. After drying for 1 week in high vacuum ($p < 10^{-8}$ bar) at 40 °C, the water content was found to be 420 ppm. All dried ILs were stored and handled in a nitrogen-filled glovebox.

2.2. Dielectric Spectroscopy. Dielectric spectroscopy measures the polarization of a sample induced by an external time-dependent electric field, $\vec{E}(t)$. This response is usually expressed as the frequency-dependent complex permittivity, $\hat{\varepsilon}(\nu)$

$$\hat{\varepsilon}(\nu) = \varepsilon'(\nu) - i\varepsilon''(\nu) \tag{1}$$

and contains contributions from rotational, vibrational, and translational motions.[21,22] The relative permittivity, $\varepsilon'(\nu)$, shows a dispersion from the static permittivity, $\varepsilon_s = \lim_{\nu\to 0}\varepsilon'(\nu)$, to the permittivity at infinite frequency, $\varepsilon_\infty = \lim_{\nu\to\infty}\varepsilon'(\nu)$. The dielectric loss, $\varepsilon''(\nu)$, describes the dissipation of energy within the sample arising from the coupling of $\vec{E}(t)$ to dipole fluctuations.

Dielectric measurements were performed using an Agilent E8364B Vector Network Analyzer (VNA) combined with two reflection probes (85070E-020 and -050) operating in the frequency ranges $0.2 \leq \nu/GHz \leq 20$ and $1 \leq \nu/GHz \leq 50$, respectively,[19] and a waveguide interferometer covering the frequencies $60 \leq \nu/GHz \leq 89$.[23] Air, mercury, and *N*,*N*-dimethylacetamide were used, respectively, as open, short, and load standards for the calibration of the VNA setup. Raw VNA data were corrected for calibration errors with a Padé approximation using purified benzonitrile and 1-butanol as secondary calibration standards.[24] The VNA data were cross-checked in the range $27 \leq \nu/GHz \leq 40$ using a waveguide transmission cell mounted to the VNA. All DRS experiments were carried out from 5 to 65 °C in 10 °C steps, with an overall temperature stability and accuracy of ±0.05 °C. For PAN, additional low-frequency (0.05 to 0.5 GHz) dielectric measurements were performed at 5, 15, and 25 °C using the cutoff type reflection cell described elsewhere.[23]

Data in the terahertz region were collected using a transmission/reflection time-domain terahertz spectrometer (THz-TDS)[25] (at Freiburg), a Bruker Vertex 70 FTIR spectrometer[17] for EAN and a Bruker IFS 66v FTIR for PAN (at Glasgow). The THz-TDS instrument covered the frequency range $0.3 \leq \nu/THz \leq 3$ and the others $0.9 \leq \nu/THz \leq 12$, respectively. Far-infrared (FIR) absorbance data were converted to complex permittivities using the Kramers−Kronig relation as described elsewhere.[26] Both THz and FIR spectra were measured from 5 to 65 °C in 20 °C steps with a temperature stability of ±0.5 C. Combination of all of these data provided dielectric spectra covering the frequency range $0.2 \leq \nu/GHz \leq 10\,000$. Additionally, THz-TDS and FTIR measurements of d_3-EAN were performed at 25 °C between 25 and 450 cm^{-1} ($0.7 \lesssim \nu/THz \lesssim 13$).

For electrically conducting samples like ILs, it is necessary for the data analysis to remove the contribution to the measured spectra due to the steady-state (the direct current, dc) movement of ions in the applied electric field. This is achieved by subtracting the Ohmic loss from the experimentally accessible total loss, $\eta''(\nu)$

$$\varepsilon''(\nu) = \eta''(\nu) - \frac{\kappa}{2\pi\nu\varepsilon_0} \tag{2}$$

where κ is the dc conductivity of the sample and ε_0 is the permittivity of free space.[22,27,28]

Conductivity corrections can be determined either by direct measurement at low frequencies or by treating κ as an additional adjustable parameter in the fitting procedure. Because of fringing field effects caused by the geometry of the VNA probes, fitted conductivities differ slightly from experimental values. Thus, measured κ values were used as a starting approximation for the conductivity correction but were adjusted to obtain the best fit. The corrected conductivities differed from the experimental values by ∼2−16%.

2.3. OKE Spectroscopy. In optical Kerr-effect spectroscopy, the dynamics of the polarizability anisotropy response of the system are observed. This response is represented by the time derivative of the two-point time-correlation function of the anisotropic part of the many-body polarizability tensor, Π[29]

$$S_{OKE}(t) \propto \frac{1}{k_B T}\frac{d}{dt}\langle \Pi_{xy}(t)\Pi_{xy}(0)\rangle \tag{3}$$

dx.doi.org/10.1021/jp502935t | J. Phys. Chem. B 2015, 119, 8826−8841

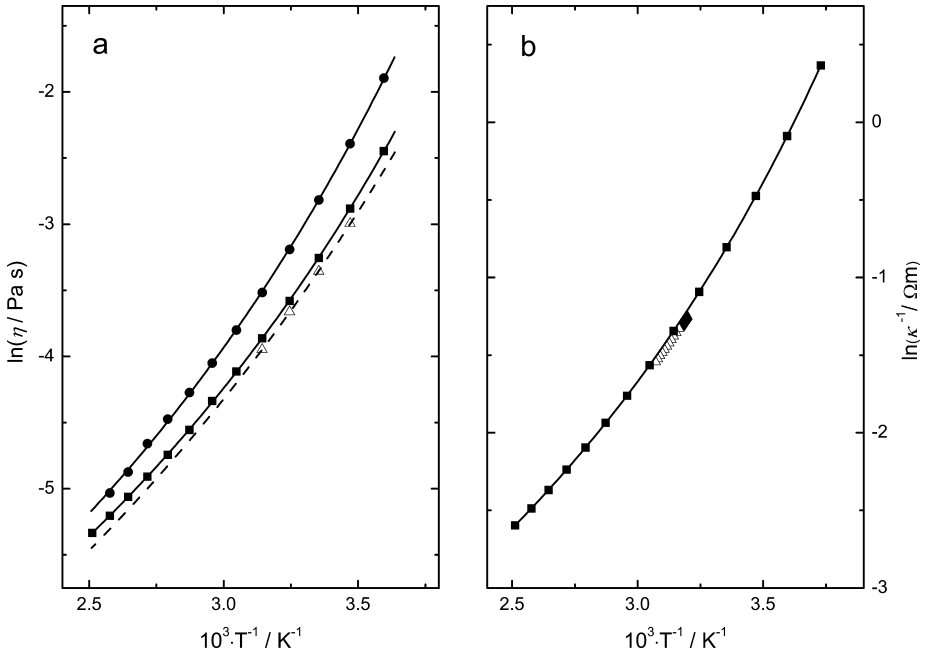

Figure 1. Present results for the physical properties of EAN (■) and PAN (●) as functions of temperature, T: (a) viscosity, η, and (b) electrical resistivity, κ^{-1}. Also included are literature data[15,36] (△) and fits with eq 6 (lines).

where k_B is Boltzmann's constant and T is the Kelvin temperature. Two OKE setups were employed to capture the full-time span of the orientational and intermolecular dynamics of EAN. For the faster dynamics, a Coherent Mira-SEED oscillator was used that generated 800 nm pulses with an energy of 8 nJ and a pulse duration of 20 fs at a repetition rate of 76 MHz. The parent beam was split into 80%-pump and 20%-probe beams, which were cofocused into a quartz cuvette containing the sample. For lower temperatures, the sample was controlled to ±0.1 °C by a cryostat (Oxford Instruments, DN). Above room temperature, a home-built copper heating block with a temperature stability of ±0.1 °C was employed. A 600 mm delay line, with a resolution of 50 nm (0.33 fs), gave a time scale of 4 ns, resulting in a bandwidth of ca. 250 MHz.[71] For slower dynamics, a similar setup using a regeneratively amplified laser (Coherent Legend USX) with a stretched pulse duration of ∼1 ps was used to increase the signal-to-noise ratio of the weak relaxation signal at longer times. The two time-domain signals were concatenated, Fourier-transformed to the frequency domain, and deconvoluted from the instantaneous response,[18] to yield the final OKE spectra.

2.4. Physical Properties. Densities, ρ, were measured from 15 (EAN) or 5 °C (PAN) to 65 °C in 10 °C steps using a vibrating-tube densimeter (Anton Paar, Graz, Austria, DMA 5000 M) with a temperature stability of ±0.01 C and a precision of $\pm 5 \times 10^{-6}$ g cm^{-3} using the calibration supplied by the manufacturer. Viscosities, η, were determined with a reproducibility of ∼0.5% using an automated rolling ball microviscometer (Anton Paar, Graz, Austria, AMVn). These measurements covered temperatures from 5 to 125 °C in 10 °C steps with an uncertainty of ±0.05 °C. Electrical conductivities, κ, of EAN were measured between −5 and 125 °C (±0.005 °C) in 10 °C steps using capillary cells in conjunction with a programmable precision LCR meter (Hameg, Mainhausen, Germany, HM8118), as described elsewhere.[30] The overall relative uncertainty in κ was estimated to be ±0.5%. Because of material constraints, none of the physicochemical properties of d_3-EAN or κ(PAN) was measured.

3. RESULTS

3.1. Densities, Viscosities, and Conductivities. The data obtained for ρ and η for EAN and PAN and κ(EAN) as functions of temperature, T, are given in Table S1 of the Supporting Information (SI). The densities followed the linear relations

$$\text{EAN: } \rho/\text{kg L}^{-1} = 1.39072 - 6.05056 \times 10^{-4} \cdot T/\text{K} \quad (4)$$

$$\text{PAN: } \rho/\text{kg L}^{-1} = 1.32833 - 5.95470 \times 10^{-4} \cdot T/\text{K} \quad (5)$$

over the temperature range investigated. The EAN results are in good agreement (∼0.1%) with the data of Weingärtner et al.[15] but differ by ∼0.5 and ∼0.7%, respectively, from those of Greaves et al.[31] and Poole et al.[32,33] For ρ(PAN) at 25 °C, the only temperature where comparison is possible, the present value is in only modest agreement with the results of Greaves et al.[1] (∼0.5%) and Atkin et al.[34] (∼0.8%).

The effects of temperature on η (and for EAN, κ, expressed as the resistivity, κ^{-1}) are displayed in logarithmic form in Figure 1. The present viscosities of EAN are systematically higher than those reported in the literature. At 25 °C, where the most extensive comparison can be made, the literature values are 34.9,[15] 26.9,[32] 32.1[33] and 36 mPa s[35] compared with the present result of 38.6 mPa s (Table S1 in the Supporting Information). This may reflect a lower water content in our material. Consistent with this inference, the temperature dependence of the present viscosities is almost identical (Figure 1a) to that of Weingärtner et al.[15] The present electrical conductivities of EAN are in reasonable agreement (∼3%) with the values reported (over a much smaller temperature range) by Oleinikova et al.[36] (Figure 1b).

The viscosities of EAN and PAN and the electrical conductivities of EAN follow the Vogel−Fulcher−Tammann (VFT) equation[37]

dx.doi.org/10.1021/jp502935t | J. Phys. Chem. B 2015, 119, 8826−8841

$$\ln Y = \ln Y_0 + \frac{B_{VFT}}{T - T_0} \quad (6)$$

where $Y = \eta$ or κ^{-1}, which is commonly used to describe the temperature dependence of transport properties of glass-forming liquids above their glass-transition temperature, T_g.[37,38] In eq 6, Y_0, B_{VFT}, and T_0 (the so-called Vogel temperature) are fitting parameters. The fit results are listed in Table S2 in the Supporting Information along with corresponding literature data.[15,36] The present values of the so-called fragility parameter, B_{VFT}, of EAN are in only modest agreement with those of Weingärtner et al.[15] and Oleinikova et al.[36] for the viscosities, although the T_0 values agree well. Because T_0 is usually ~30 K below T_g,[38] the present value of T_0 = 147.65 K for EAN is also consistent with the result of T_g = 181.65 K reported by Belieres et al.[35] The present VFT parameters of PAN are broadly compatible with those of Smith et al.[39] but less so with those of Bouzón Capelo et al.[40]

3.2. Spectroscopic Model Selection and Fitting. *General Comments.* Representative OKE and DR spectra of EAN and DR spectra of PAN over the frequency range: 200 MHz $\leq \nu \leq$ 10 THz at temperatures from (5 to 65) °C are presented in Figures 2−4, respectively. OKE spectra of PAN

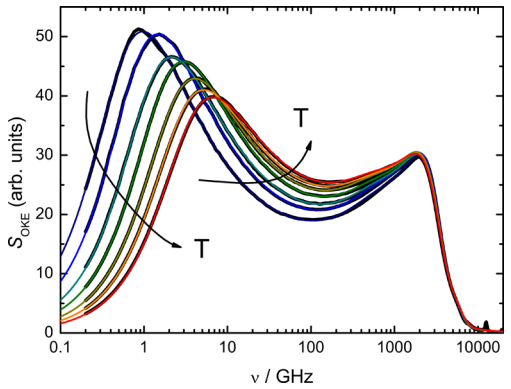

Figure 2. Optical Kerr-effect spectra of EAN from 5 to 65 °C in 10 C steps. Black circles are resampled experimental data; overlaying colored lines represent the total fit.

are reported elsewhere.[18] It should be stressed that the dielectric spectra were resampled (i.e., linearly interpolated) prior to fitting. This was necessary to achieve an equal point density over the entire frequency range and to stabilize the fit of the small intensities at high frequencies.

An appropriate mathematical description of the experimental data is necessary to understand the spectra on a molecular level. This was achieved by fitting $\hat{\varepsilon}(\nu)$ or the frequency-dependent OKE response, $S_{OKE}(\nu)$, with a sum of n individual processes of band-shape function $\tilde{F}_j(\nu)$ and amplitude S_j

$$y = \sum_{j=1}^{n} S_j \cdot \tilde{F}(\nu) + y_\infty \quad (7)$$

where $y = \hat{\varepsilon}(\nu)$ and $y_\infty = \varepsilon_\infty$ for DR and $y = S_{OKE}(\nu)$ and $y_\infty = 0$ for OKE spectra. Lower-frequency modes ($\lesssim$ 100 GHz) associated with molecular reorientations were modeled using relaxation functions, whereas librations and intermolecular vibrations in the terahertz region were better modeled as resonances.[28] However, before describing the model ultimately selected, it is important to recognize that fitting DR and OKE spectra over such a broad frequency range is a formidable task that cannot be performed ab initio. It therefore follows that any mathematical description adopted invariably involves some degree of choice. Because the fitting of the spectra is critical to their interpretation, it is appropriate to discuss now this aspect of the present work in some detail.

Difficulties in Fitting OKE and DR Spectra. The major difficulties in fitting the present spectra can be summarized as follows. First, resonance and especially relaxation modes are often broad and generally strongly overlapping. Second, there are certain theoretical and computational problems associated with some of the standard mathematical models used to describe the modes, see later. Third, the present (in particular, the DR) spectra exhibit a broad featureless and low (but finite) intensity over the intermediate frequency range 0.05 $\lesssim \nu$/THz $\lesssim$ 1 (Figures 2−6), which is particularly hard to model. Fourth, the accuracy of the spectra is limited by the unwanted conductivity contribution (eq 2), which swamps the DR (but not the OKE) signal at low frequencies (say, $\nu \lesssim$ 0.5 GHz), and by current technological limitations on the accuracy of the apparatus at higher frequencies (say, $\nu \gtrsim$ 100 GHz). Lastly, there are no a priori guidelines that limit the number or nature of the modes present; this is especially critical because the modes are expected to be strongly coupled and overlapping.[41] These effects are important in DR and OKE spectroscopy because both techniques probe collective dynamics. Such spectra therefore reflect not only the motions of individual molecules and ions but also coupling effects. Furthermore, in ILs, not only are the motions of the various species coupled but also their translational and rotational motions are not independent of each other. In particular, it is well-known from simulations that rotation-translation cross-correlations may yield negative contributions to IL spectra.[42−45] Unfortunately, up until now, computer simulations have only been able to provide, at best, qualitative descriptions of experimental DR and OKE spectra.[46] For this reason, the standard spectroscopic approach, based on eq 7 and described in detail later, is still the best available for a qualitative description of the spectra. Accordingly, this approach will now be described in detail.

For relaxation processes, which usually appear at lower frequencies ($\lesssim$100 GHz), the empirical Havriliak−Negami (HN) equation of band shape $\tilde{F}_{HN}$ is suitable. For reasons described in detail elsewhere,[18,17] this equation was used in its inertia-corrected form (HNi)

$$\tilde{F}_{HNi}(\nu) = (S^0_{HNi})^{-1}\left[\frac{1}{(1 + (i2\pi\nu\tau)^{1-\alpha})^\beta} - \frac{1}{(1 + (i2\pi\nu\tau + \gamma_{lib}\tau)^{1-\alpha})^\beta}\right] \quad (8)$$

where τ is the relaxation time, γ_{lib} is the inertial rise rate, α and β are the width parameters, and S^0_{HNi} is the amplitude normalization factor

$$S^0_{HNi} = 1 - \frac{1}{(1 + (\gamma_{lib}\tau)^{1-\alpha})^\beta} \quad (9)$$

The limiting forms of the Havriliak−Negami equation are the Cole−Davidson (CD, $\alpha_j = 0$), Cole−Cole (CC, $\beta_j = 1$), and Debye (D, $\alpha_j = 0$, $\beta_j = 1$) equations and their inertia-corrected versions CDi, CCi, and Di.[47]

The higher-frequency (terahertz and FIR) region is dominated mainly by librational motions and low-energy inter- and intramolecular vibrations. Such processes are best represented by a resonance-type band-shape function such as a damped harmonic (Brownian) oscillator (DHO)[48]

dx.doi.org/10.1021/jp502935t | J. Phys. Chem. B 2015, 119, 8826−8841

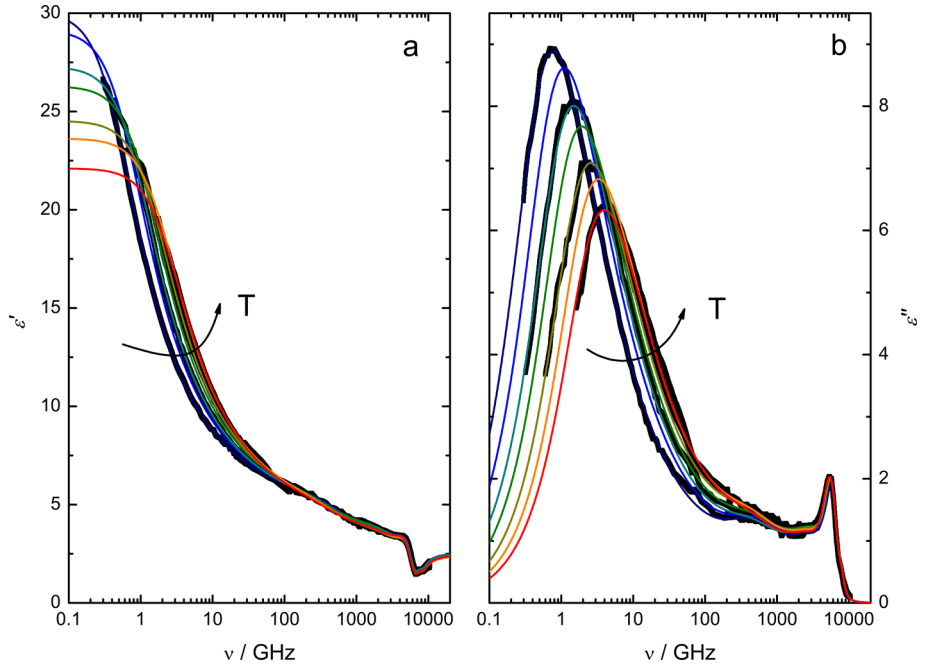

Figure 3. (a) Permittivity, $\varepsilon'(\nu)$, and (b) dielectric loss, $\varepsilon''(\nu)$, spectra of EAN from 5 to 65 °C in 10 °C steps. For visual clarity, data at 15, 35, and 55 °C are not displayed. Black squares are resampled experimental data; overlaying colored lines represent the overall fit.

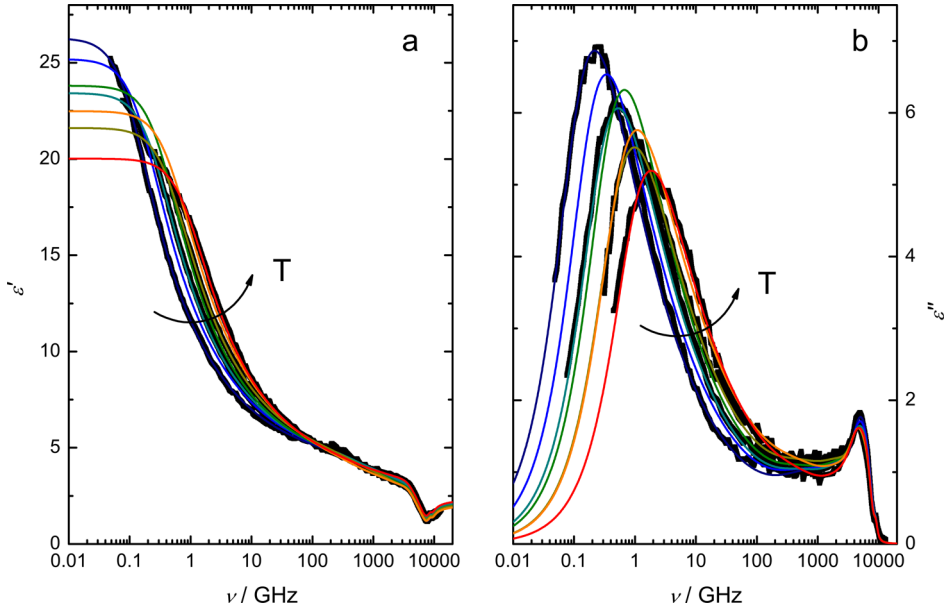

Figure 4. (a) Permittivity, $\varepsilon'(\nu)$, and (b) dielectric loss, $\varepsilon''(\nu)$, spectra of PAN from 5 to 65 °C in 10 °C steps. For visual clarity, data at 15, 35, and 55 °C are not displayed. Black squares are resampled experimental data; overlaying colored lines represent the overall fit.

$$\tilde{F}_{\mathrm{DHO}}(\nu) = \frac{\nu_0^2}{(\nu_0^2 - \nu^2) + \mathrm{i}\nu\gamma_{\mathrm{DHO}}} \tag{10}$$

with resonance frequency, ν_0, and damping constant, γ_{DHO}. Alternatively, an antisymmetrized Gaussian oscillator (G)

$$\tilde{F}_{\mathrm{G}}(\nu) = (S_{\mathrm{G}}^0)^{-1}\left[\frac{2}{\sqrt{\pi}} \times \mathrm{Da}\left(\frac{\nu + \nu_0}{\sqrt{2}\gamma_{\mathrm{G}}}\right) - \frac{2}{\sqrt{\pi}} \times \mathrm{Da}\left(\frac{\nu - \nu_0}{\sqrt{2}\gamma_{\mathrm{G}}}\right) + i\left(\exp\left[-\frac{(\nu - \nu_0)^2}{2\gamma_{\mathrm{G}}^2}\right] - \exp\left[-\frac{(\nu + \nu_0)^2}{2\gamma_{\mathrm{G}}^2}\right]\right)\right] \tag{11}$$

with resonance frequency, ν_0, and half bandwidth, γ_{G}, can be used where

$$S_{\mathrm{G}}^0 = \frac{4}{\sqrt{\pi}} \times \mathrm{Da}\left(\frac{\nu_0}{\sqrt{2}\gamma_{\mathrm{G}}}\right) \tag{12}$$

Note that in eqs 11 and 12, $\mathrm{Da}(x)$ is Dawson's integral[49] and S_{G}^0 is the amplitude normalization factor for this band-shape function.

Adopted Fitting Approach. Bearing in mind the difficulties previously discussed, after an extensive investigation of the possibilities, the following description (presented as five dot points) was adopted for fitting the OKE and DR spectra of

dx.doi.org/10.1021/jp502935t | J. Phys. Chem. B 2015, 119, 8826−8841

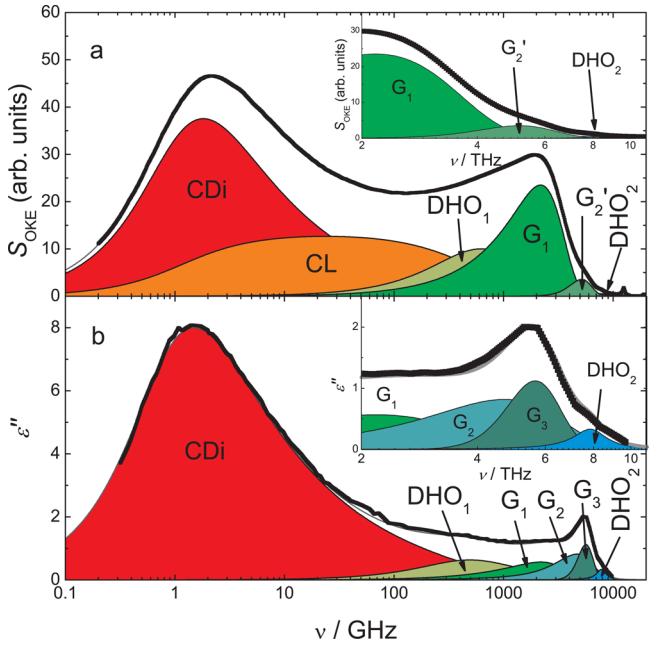

Figure 5. Imaginary part of (a) OKE and (b) DR spectra of EAN at 25 °C. Black squares are resampled experimental data, and thin gray lines represent the overall fit. Shaded areas indicate the contributions of the individual processes assuming a (CDi + CL + DHO_1 + G_1 + G_2' + DHO_2) model for the OKE spectrum and a (CDi + DHO_1 + G_1 + G_2 + G_3 + DHO_2) model for the DR spectrum. Insets: expanded views of the high frequency data.

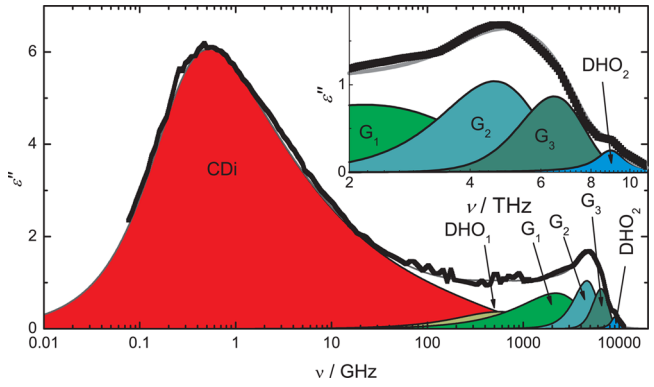

Figure 6. Dielectric loss spectrum of PAN at 25 °C. Black squares are resampled experimental data, and the gray line represents the overall fit of the (CDi + DHO_1 + G_1 + G_2 + G_3 + DHO_2) model. Shaded areas indicate the contributions of the individual processes. Inset: expanded view of high-frequency data.

EAN. As will be shown, this description was also found to be applicable without modification to d_3-EAN (Section 5.2) and PAN (Section 5.3).

•The broad-band OKE and DR spectra of EAN at all temperatures (Figures 2 and 3) show two clear features: a dominant temperature-dependent relaxation in the low gigahertz region and a much narrower almost temperature-independent resonance process in the terahertz region. The dominant low gigahertz process is the so-called α-relaxation,[18,50] which was found to be best described by an inertia-corrected Cole−Davidson (CDi) function (eq 8 with $\alpha_{CDi} = 0$). For stabilization of the fits of the DR spectra, the width parameter, β, was fixed at 0.5 for all temperatures, as it varied only slightly with T when allowed to float. Note that an asymmetrical (i.e., a CD) band shape, broadened to higher frequencies, was preferred over the symmetrically broadened (CC) function used for other ILs[50] because the low-frequency wing of the α-mode of EAN exhibited a Debye rather than a broadened, band shape (Figure 5). The high-frequency (inertial) termination of the α-relaxation was achieved by fixing γ_{lib} at 3 and 5 THz for the fits of the OKE and DR spectra, respectively.

•As discussed elsewhere,[18] the featureless intensity of the OKE spectrum in the intermediate frequency range $50 \lesssim \nu/\mathrm{GHz} \lesssim 1000$ (i.e., "intermediate" between the α-relaxation and the higher frequency librational modes) was approximated by a modified Cole−Cole function (CCm). In the limit of $\alpha_{CCm} \rightarrow 1$, this contribution appears as a constant loss (CL),[18] which corresponds to a logarithmic decay in the time domain, which is typical for glass-forming liquids.[51] The CL contribution was made compatible with the spectroscopic dynamics in the intermediate region by the application of an inertial correction at high frequencies and a so-called α-termination at low frequencies.[18] This CL "mode" is undoubtedly a composite, but little can be said in this stage about the nature or relative contributions of the processes that produce it.

In the course of reanalyzing the high-frequency parts of the OKE and DR spectra, it was found to be necessary to modify slightly the previous[18] fit model. In doing so, it turned out that the CL contribution, which is indispensable for describing the OKE spectra,[18] can be neglected in the DR spectra. This is because the amplitude of this contribution is much smaller in the latter; in addition, the inclusion of a CL contribution did not improve the fit either in the rather poorly defined region near 100 GHz or overall in terms of the normalized variance of the fit, χ_r^2. Furthermore, application of the CL term to the DR spectra of PAN produced physically impossible negative values of the CL amplitude, S_{CL}. These findings do not prove the absence of a CL contribution to the DR spectra; more likely, it is subsumed in the neighboring CDi and DHO_1 modes. Removal of the CL contribution in all DR spectra reduced the number of fitting parameters without affecting χ_r^2, consistent with the usual criteria for model selection.[52]

•While there was no explicit indication of a mode at ∼1 THz in the present spectra of EAN (Figures 2 and 3), OKE measurements at low T clearly indicated the existence of such a mode for PAN.[18] Accordingly, an analogous mode, DHO_1, was assumed for EAN, which considerably improved χ_r^2.

•At $\nu > 1$ THz, both OKE and DR spectra of EAN were dominated by apparent modes at ∼2 THz (Figures 2 and 5a) and ∼5.5 THz (Figures 3 and 5b), respectively. To account for the observed intensities in this frequency range, Gaussians were preferred over DHOs because they better described the steep decay of the OKE and $\varepsilon''(\nu)$ intensities at $5.5 \lesssim /\mathrm{THz} \lesssim 7.2$. It was further established that the intensity in this region of the OKE spectra was best described by a large-amplitude Gaussian, G_1, centered at ∼2 THz and a second weaker Gaussian, G_2', that accounted for the poorly defined shoulder at ∼5 THz (Figures 2 and 5a). For the DR spectra (Figure 5b), the G_1 mode was again required; however, while a G_2' mode at ∼5.5 THz provided reasonable fits,[18] considerable improvement was achieved by splitting it into two Gaussians, G_2 and G_3. Support for the existence of an additional process comes from the DR spectra of PAN, which show a small but distinct shoulder at ∼6.5 THz (Figure 6 inset). These findings, in turn, suggest that the G_2' mode in the OKE spectra (Figure 5a) is almost certainly

dx.doi.org/10.1021/jp502935t | J. Phys. Chem. B 2015, 119, 8826−8841

a composite, consistent with its resonance frequency lying between those of G_2 and G_3 in the DR spectra.

•To account for the remaining intensity at the highest frequencies in the DR and OKE spectra: a poorly defined shoulder in EAN (Figure 5 insets) and a small peak in the PAN spectrum (Figure 6 inset), it was necessary to include a mode, DHO_2, corresponding to the intramolecular mode reported by Fumino et al.[13] at 7.9 THz (263.3 cm^{-1}) in the FIR spectrum of EAN. The resonance frequency of this mode was fixed at 7.9 THz, and its amplitude, S_{DHO_2}, and damping constant, γ_{DHO_2}, were arbitrarily set to the values listed in Tables S3 and S4 in the Supporting Information to achieve convergence.

Thus, the models adopted as providing the best description of the spectra over the extraordinarily wide range of frequencies used in this study were, for OKE, (CDi + CL + DHO_1 + G_1 + G_2' + DHO_2), and for DR, (CDi + DHO_1 + G_1 + G_2 + G_3 + DHO_2). The overall fits obtained at 25 °C are shown in Figure 5a (OKE) and Figure 5b (DR). Similar fits (not shown) were obtained for the OKE and DR spectra at 5, 45, and 65 °C, and the parameters so derived are summarized in Tables S3 and S4 in the Supporting Information. Note, however, that because of the absence of THz-TDS and FIR data at 15, 35, and 55 °C, parameters for the resonance modes (DHO_1, G_1, G_2 and G_3) at these temperatures, also listed for convenience in Tables S3 and S4 in the Supporting Information, were obtained by linear interpolation.

Fitting of d_3-EAN and PAN Spectra. The DR and OKE spectra of d_3-EAN at 25 °C were well-fitted with the models used for EAN with fixed values of: γ_{lib} = 5 THz and ν_{0,DHO_2} = 7.7 THz (Figure S1 in the Supporting Information). The model used for EAN also provided a fully satisfactory fit for the DR spectra of PAN at the temperatures studied (Figure 6). The derived parameters are listed in Table S5 in the Supporting Information, noting that as for EAN the parameters of the resonance modes (DHO_1, G_1, G_2, and G_3) at 15, 35, and 55 °C were obtained by linear interpolation. The resonance frequency of the DHO_2 mode, ν_{0,DHO_2}, in PAN was fixed at 9.0 THz consistent with that reported by Fumino et al.,[13] and its amplitude, S_{DHO_2}, and damping constant, γ_{DHO_2}, were set arbitrarily to the values listed in Table S5 in the Supporting Information to achieve convergence. The inertial rise rate, γ_{lib}, was fixed at 5 THz. For a fuller discussion of the OKE spectra of PAN, the reader is referred to ref 53.

Comparison of the DR spectra of EAN and PAN (Figures 3 and 4) revealed that the latter were significantly more scattered over the entire frequency range. In particular, the increased noise in the THz-TDS data exacerbated an unambiguous concatenation of the FIR and lower frequency spectra. This introduced additional uncertainties into the fit of the intermediate and high-frequency regions of the PAN spectra; nevertheless, the fit parameters so obtained are broadly consistent with the EAN data (Section 5.3).

4. DISCUSSION OF "SLOW" DYNAMICS ($\nu \lesssim$ 100 GHz)

4.1. Static Permittivity. Before going on to discuss the details of the modes identified in the OKE and DR spectra at $\nu \lesssim$ 100 GHz, it is appropriate to consider the behavior of the latter in the low-frequency limit. Dielectric spectroscopy is the only experimental method currently available for measuring the static permittivity (dielectric constant) of a conducting liquid.[22] The values of the static permittivity ($\varepsilon_s = \lim_{\nu\to 0}\varepsilon'(\nu) = \sum_j S_j + \varepsilon_\infty$) obtained for EAN and PAN from the fits of the present DR spectra are shown as a function of temperature in Figure 7. As

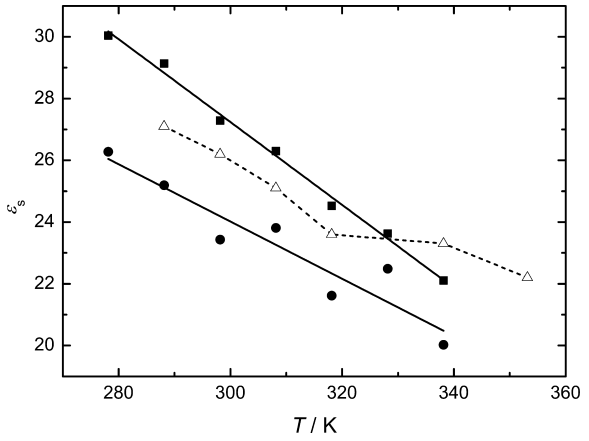

Figure 7. Present results for the static permittivity, ε_s, of EAN (■) and PAN (●) as a function of temperature; solid lines are linear regressions of the present data; open triangles (△) show the EAN values of Weingärtner et al.[15]

for other ILs,[50] ε_s exhibits a monotonic (in fact approximately linear) decrease with increasing temperature, with $d\varepsilon_s/dT$ = −0.13 K^{-1} (EAN) or −0.09 K^{-1} (PAN). These large negative values of $d\varepsilon_s/dT$ are about three times greater than for typical aprotic ILs[50] but are similar to those of H-bonded molecular liquids such as alcohols, where they are ascribed to a partial breakup of the H-bond networks with increasing T. As would be expected from their protic character, the values of $\varepsilon_s \approx$ 27.3 (EAN) and 23.4 (PAN) at 25 °C are considerably higher than those observed for aprotic ILs, which are typically <20.[50,54] It should be noted in passing that there is some uncertainty in the determination of ε_s for both EAN and PAN. This is because the dominant α-relaxation (Section 4.2) slows down considerably (shifts to lower frequencies) at lower T, which means that $\varepsilon'(\nu)$ does not reach its plateau within the accessible frequency range (Figures 3a and 4a). Measurements at lower ν do not help because the dielectric signal is swamped by the conductivity contribution (eq 2). These difficulties, and the limited accuracy of existing dielectric instrumentation, readily account for the small differences (ca. 3−5%) between the present values of ε_s and of $d\varepsilon_s/dT$ for EAN and those of Weingärtner et al.[15] (Figure 7).

4.2. α-Relaxation Process. *General Aspects.* The dominant process in both the DR and OKE spectra of EAN and PAN in the low gigahertz region (Figures 2−6) is the so-called α-relaxation,[53] which corresponds to the structural relaxation of (rotational motions of molecular-level species in) each liquid.[21] Because of its three-fold symmetry axis, the nitrate anion has a zero dipole moment and thus will make no direct contribution to the DR spectra. Because of its π electrons, NO_3^- is highly polarizable and due to its planar geometry, it has a high anisotropy ($\alpha_\parallel \approx$ 5.6 Å^3, $\alpha_\perp \approx$ 3.1 Å^3)[55] so that the motions of NO_3^- will therefore be a major contributor to the OKE spectra. Conversely, the ethyl- and propylammonium cations ($EtNH_3^+$ and $PrNH_3^+$) are only weakly polarizable and anisotropic but have considerable permanent dipole moments ($\mu \approx$ 3.9 and 6.8 D, respectively, from MOPAC calculations[56]), which make them significant contributors to the dielectric signal. In this sense, EAN and

dx.doi.org/10.1021/jp502935t | J. Phys. Chem. B 2015, 119, 8826−8841

PAN can be viewed as almost perfect compounds for complementary investigation by OKE and DR spectroscopies.[18]

The amplitude of the α-relaxation decreased considerably with increasing T in both the OKE and DR spectra (Figures 2 and 3). Furthermore, the peak maximum shifted from 0.8 to 6 GHz in the OKE spectra (0.7 to 4 GHz in the DR spectra) for EAN (Figures 2 and 3) and from 0.2 to 2 GHz in the DR spectra of PAN (Figure 4) over the studied temperature range. These features of the α-relaxation are broadly similar to those observed for the corresponding process in imidazolium-based ILs,[17] although, as would be expected, there is no evidence in the present ILs of a sub-α process, which is thought to be a breathing mode of π-stacked cation aggregates.[17]

Relaxation Times. The relaxation times of the α-process, τ_α, in the DR and OKE spectra of EAN and PAN decrease exponentially with increasing T, thus permitting application of the Arrhenius equation. As already noted (Section 3.1), the viscosities of both liquids follow the VFT relation over the same temperature range. As a consequence, Stokes−Einstein−Debye (SED) plots of τ_α^{DR}(EAN), τ_α^{OKE}(EAN), and τ_α^{DR}(PAN) against η/k_BT depart from linearity at low T[18] (for convenience, these plots are reproduced in Figure S2 in the Supporting Information), which implies a decoupling of the molecular-level rotational motions from the bulk viscosity. At higher T, the effective volumes of rotation, V_{eff}, extracted from the slopes of the SED plots were rather small and were not compatible with the probable rotational motions of the anions (out-of-plane rotation for NO_3^-) or the cations (end-over-end rotation for RNH_3^+).[18] The nonlinearity of the SED plots is instead consistent with a high degree of rotational cooperativity between the anions and cations, rather than the simple independent rotational diffusion assumed in the SED theory.

For EAN, further evidence of such cooperative motions comes from a comparison of DRS with time-resolved femtosecond-IR spectroscopy (fs-IRS).[57] As fs-IRS probes the rotation of the N−H bonds, it is also sensitive to the rotations of the $EtNH_3^+$ cation, which manifests itself in an activation energy (E_A^{IR} = 21.4 ± 0.6 kJ mol^{-1})[57] that is virtually identical with the present results (E_A^{DR} = 21.6 ± 0.3 kJ mol^{-1}). Within the rotational diffusion model, where specific interactions of the rotating entity with its surroundings are ignored, a ratio of $\tau_{\alpha,max}^{DR}/\tau^{IR}$ = 3 is expected as the fs-IR relaxation times, τ^{IR}, are of second rank in contrast with the first-rank relaxation time, τ_α^{DR}, measured via DRS.[28] For EAN, the observed ratio has an average value of 1.4,[58] which is consistent with the α-relaxation process occurring via a jump mechanism, as previously proposed for aprotic ILs,[17,59] rather than through rotational diffusion. In water, where molecular reorientation is also thought to take place via large-angle jumps,[60] the ratio of first- to second-rank rotational correlation times is ∼2, from which it was concluded that the relaxation rate in water is determined by the rate of H-bond breaking.[61] It seems likely that this is also the case in EAN, with the even lower value of $\tau_{\alpha,max}^{DR}/\tau^{IR}$ reflecting the very strong and multiple cation−anion H-bond interactions. Knowledge of the ratio $\tau_{\alpha,max}^{DR}/\tau^{IR}$ permits[57] calculation of the jump angle, yielding a result of 106°. This value is almost identical with the tetrahedral angle of the ammonium group, which is again consistent with strong, directed H-bond interactions between $EtNH_3^+$ and NO_3^-.

This conclusion is further supported by the similarity of the activation energies for both EAN and PAN obtained from the temperature dependence of τ_α^{DR} (E_α^{DR}/kJ mol^{-1} = 21.6 ± 0.3 (EAN) or 26.0 ± 1.7 (PAN)) and τ_α^{OKE} (E_A^{OKE}/kJ mol^{-1} = 24.0 (EAN) or 25.5 (PAN)).[18,19] These relatively large E_A values, and particularly their similarity, indicate a high degree of cooperativity between the rotating species and their neighbors. Such cooperativity is also implied by the similarity of τ_α^{DR} and τ_α^{OKE} at all T, which suggests that anion dynamics are slowed down to the time scale of cation reorientation as a result of strong interionic interactions.

Amplitudes. The amplitudes (intensities) of the α-relaxation in the DR spectra, S_α^{DR}, arise from the motions of the dipolar species present. In a PIL, these include cooperative fluctuations of the H-bond network, including H-bond making and breaking. For EAN and PAN, S_α^{DR} is dominated by the rotational motions of $EtNH_3^+$ and $PrNH_3^+$, which have gas-phase dipole moments, μ = 3.86 D[62] and 6.84 D(MOPAC[56]), respectively. The NO_3^- ion has no dipole moment and thus makes no *direct* contribution to the DR spectrum. However, the translational motions of the ions will contribute in this frequency range,[46] as well as the rotational/translational motions of any ion pairs (IPs) or larger clusters that have $\mu \neq 0$ and an appropriate lifetime. The corresponding OKE amplitude, S_α^{OKE}, arises from changes in polarizability anisotropy, which, as argued above in this Section, mainly reflects the motions of the NO_3^- ion, along with any IPs or larger clusters containing NO_3^- that have the relevant characteristics. Note that, as with all neat ILs investigated to date,[50] there is no evidence in the DR spectra of the existence of discrete IPs in the present PILs; furthermore, any larger clusters (if present) that might be detected by DR and OKE will not necessarily be identical. Nor is it known a priori what are the relative contributions to S_α arising from the ions, IPs and (if present) clusters.

Quantitative evaluation of S_α^{DR} was made via the equation (where N_A is Avogadro's constant)

$$\frac{\varepsilon_s + A_j(1-\varepsilon_s)}{\varepsilon_s}\cdot S_j = \frac{N_A c_j}{3k_BT\varepsilon_0}\cdot\mu_{eff,j}^2 \qquad (13)$$

which relates the amplitude of a relaxation process, S_j, to the effective dipole moment, $\mu_{eff,j}$, of the relaxing species j of concentration, c_j.[63] To apply eq 13, the shapes of $EtNH_3^+$ and $PrNH_3^+$ were approximated as prolate ellipsoids using the equations for the geometric factor, A_j, given by Scholte.[64] The values of μ_{eff} so obtained decrease linearly with increasing T (Figure 8).

Within the likely experimental errors, the present μ_{eff} values agree well with those of Weingärtner et al.[15] up to 45 °C, although the latter's values at 65 and 80 °C differ significantly from the trend of the present results. For EAN, μ_{eff} coincides with the apparent dipole moment, μ_{app} = 4.9 D, of $EtNH_3^+$ calculated by MOPAC,[56] consistent with the assumption that S_α^{DR} mostly arises from cation reorientation. The value of μ_{eff} for PAN is significantly higher than that for EAN (Figure 8) consistent with its higher MOPAC-calculated value (μ_{app} = 7.9 D).[65] The decrease in μ_{eff} with increasing T contrasts with all aprotic imidazolium-based ILs studied to date, for which μ_{eff} was found to be independent of T,[50] which has been interpreted as indicating an absence of structural change. The negative values of $d\mu_{eff}/dT$ of EAN and possibly PAN (Figure 8) therefore imply increasing dipole−dipole interactions in these PILs at lower T. This is consistent with the formation of higher order clusters and perhaps also with increasing microheterogeneity, as proposed by Hayes et al.[9] Whatever the exact nature of the orientational correlations of the dipoles,

dx.doi.org/10.1021/jp502935t | J. Phys. Chem. B 2015, 119, 8826−8841

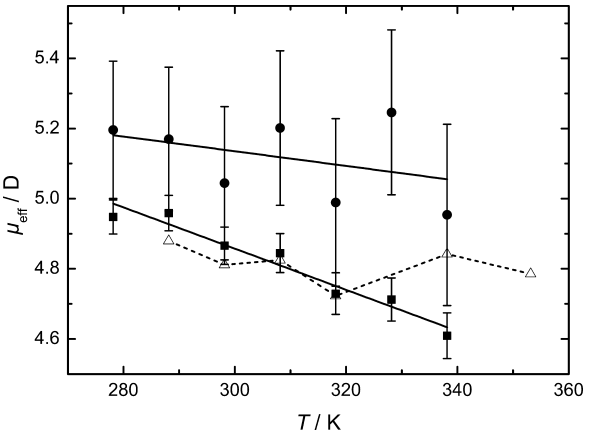

Figure 8. Present results for the effective dipole moment, μ_{eff}, of the α process as a function of temperature: EAN (■) and PAN (●). Solid lines represent linear fits of the present data; open triangles (△) are literature values for EAN.[15]

it is likely that they are also responsible for the decoupling of viscosity and rotational motions inferred from the relaxation time. The fact that ε_s(PAN) < ε_s(EAN) despite having a larger value of μ_{eff} can be reasonably ascribed to the lower dipole density in PAN.

5. DISCUSSION OF "FAST" DYNAMICS ($\nu \gtrsim 100$ GHz)

5.1. EAN. The observed intensity of the broadband DR and OKE spectra of ILs in the frequency range 0.1 < ν/THz < 13 (ca. 3 to 400 cm^{-1}) mostly arises from librations and intermolecular vibrations.[17,66,67] For PILs, low-energy intramolecular vibrations and proton transfers may also contribute. Because of the strong interionic interactions in PILs and the presumed extensive coupling and overlapping of rotational, vibrational, and translational modes,[41] unambiguous decomposition and assignment of modes in this region is especially difficult (Section 3.2). Nevertheless, the different "selection rules" for OKE, sensitive to fluctuations of the polarizability anisotropy, and DRS, probing dipole fluctuations, means that a combination of OKE and DR spectroscopies can provide valuable insights into the complicated dynamics of PILs on this time scale.

On the basis of DFT calculations of small PIL clusters, Fumino et al.[13] assigned contributions in the 50 to 400 cm^{-1} range of their FIR absorption spectra of EAN and related compounds to intermolecular H-bond bending, asymmetric and symmetric stretching (Table 1), drawing particular attention to the similarity of these modes to those observed for water. On the other hand, Winkler et al.[68] have suggested that it may not be possible to distinguish symmetric and asymmetric H-bond stretching modes in H-bonding liquids due to the fast dynamic exchange between different H-bonded configurations. Furthermore, in addition to H-bond vibrations, it is reasonable to expect that intensity in this region must also reflect the librational motions of NO_3^- and $EtNH_3^+$.

The contributions of librational motions to the OKE and DR spectra can be estimated using the free-rotator approximation of Bartoli.[69] This model predicts, based on their moments of inertia ($EtNH_3^+$: $I_B = 100.6 \times 10^{-47}$ kg m^2, $I_C = 114.4 \times 10^{-47}$ kg m^2; NO_3^-: $I_A = I_B = 61.9 \times 10^{-47}$ kg m^2),[56] that the libration frequencies of NO_3^- and $EtNH_3^+$ should be reduced by factors of ~7 and ~9, respectively, compared with water. Using the value of ~680 cm^{-1} for the libration mode of water[70] and

Table 1. Comparison for EAN of the Resonance Frequencies, $\bar{\nu}_0$/cm^{-1}, of the Present OKE and DR Modes, DHO_1, G_1, G_2, G_2', and G_3 (Intermolecular) and DHO_2 (Intramolecular) at 65 °C, with the FIR Absorption Modes Reported at 80 °C by Fumino et al.[13]

				assignment	
mode	$\bar{\nu}_0^{OKE}$	$\bar{\nu}_0^{DR}$	$\bar{\nu}_0^{FIR13}$	Fumino et al.[13a]	this work
DHO_1	49.4	49.4[b]	[c]	[c]	H-bond bending
G_1	68.4	68.4[b]	60	H-bond bending	NO_3^- librations
G_2		149.1	132	symmetric H-bond stretching	H-bond stretching
G_2'	166.1		[c]	[c]	unresolved combination of G_2 and G_3, see text
G_3		184.8	199	asymmetric H-bond stretching	RNH_3^+ librations
DHO_2	263.3	263.3	265.2	ethyl group torsion	ethyl group torsion

[a]Based on DFT calculations of small PIL clusters. [b]Fixed to that of the OKE fit. [c]Not detected.

assuming for simplicity that the same mean-square torque is acting, values of ~2.9 THz (97 cm^{-1}) for the librational motion of NO_3^- and ~2.3 THz (76 cm^{-1}) for $EtNH_3^+$ are obtained. It is therefore essential to consider possible librational contributions to the FIR spectra. A full discussion of the present assignment of the observed modes in the OKE and DR spectra that includes such contributions is given below. It is reiterated (see Section 3.2.) that the present approach is necessarily a simplified picture of PIL dynamics because in reality it is anticipated that all intermolecular motions in this (FIR) region are strongly coupled. However, as long as computer simulations and theoretical approaches are unable to provide quantitative estimates of these coupling effects, the present approach is the best available.

OKE Fits. As previously discussed, the high-frequency portion of the OKE spectra for EAN was best-fitted by a model consisting of a damped harmonic oscillator, DHO_1 (at ~1.5 THz), two Gaussians, G_1 (~2 THz), and G_2' (~5 THz), plus an additional mode (DHO_2; 7.9 THz) that accounted for the small peak in the OKE spectra (Figure 5a, inset), which also shows up in the DR spectra as a shoulder (Figure 5b, inset) and which is associated with ethyl-group torsion (Table 1).[13]

Figure 9 displays the temperature dependence of the amplitudes, bandwidths and resonance frequencies of the proposed high-frequency processes. The OKE amplitudes (Figure 9d) were only weakly affected by T: S_{G1}(▲) and $S_{G2'}$(◆) increased slightly, while S_{DHO_1}(□) was more or less constant over the investigated range. The damping constants (Figure 9e) differed significantly, with γ_{G1}(▲) and $\gamma_{G2'}$(◆) increasing with increasing T (with a larger slope for the latter), while γ_{DHO_1}(□) remained approximately constant. The OKE resonance frequencies (Figure 9f) of all processes decreased with increasing T. For librations, this decrease is generally explained by a general increase in molecular motions and weakening of the surrounding cage as the density decreases. However, these same factors also lower the force constants of intermolecular vibrations, such as H-bond bending or stretching, which would also lower ν_0 as T increases. It is therefore not possible to use these observations to determine

dx.doi.org/10.1021/jp502935t | J. Phys. Chem. B 2015, 119, 8826−8841

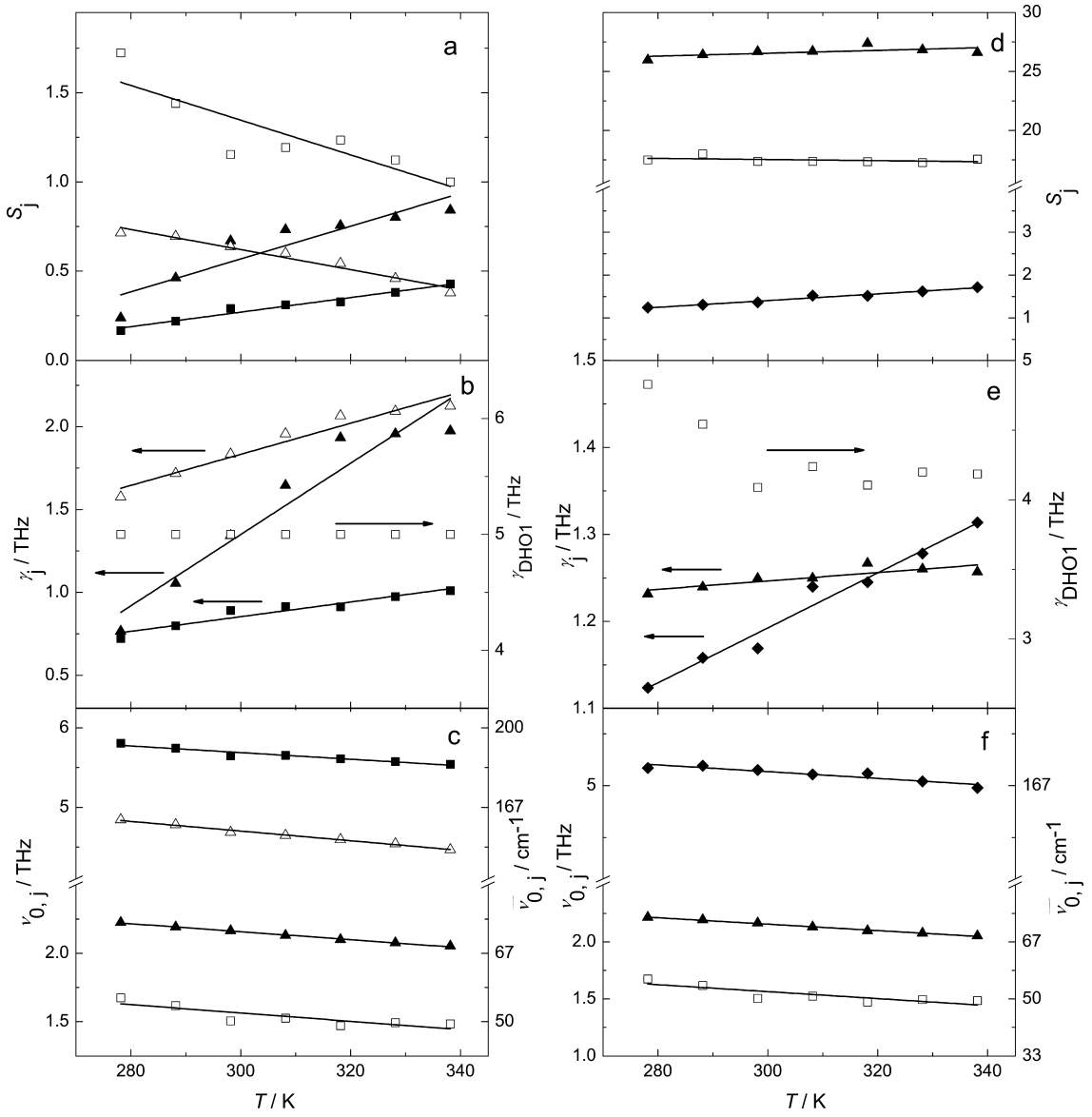

Figure 9. Fit parameters for the high-frequency resonance processes of EAN as a function of temperature: (a) amplitudes, S_j, (b) damping constants, γ_j, and (c) resonance frequencies, $\nu_{0,j}$, of the DHO_1 (□), G_1 (▲), G_2 (△), and G_3 (■) modes in the DR spectra and (d) S_j, (e) γ_j, and (f) $\nu_{0,j}$, of the DHO_1 (□), G_1 (▲), G_2' (◆) modes in the OKE spectra. Solid lines are linear regressions of the data.

whether these modes (G_1, G_2', DHO_1, and DHO_2) are librations or vibrations.

The location (Table 1) of $\overline{\nu}_{0,G1}$ in OKE spectra for EAN (68.4 cm^{-1} at 338 K) is compatible with the FIR mode at ∼60 cm^{-1} at 353 K, assigned by Fumino et al.[13] to H-bond bending. However, the present OKE measurements indicate that this mode must arise mostly from librational motions of the nitrate anion. The justifications for this assignment are as follows. First, in contrast with NO_3^-, the polarizability anisotropy of the cation is small (see Section 4.2), so the anion dominates the OKE response. Second, because OKE is primarily sensitive to rotational motions, it would not be expected to detect H-bond bending.[71] Third, the OKE spectra of all liquids show a pronounced librational peak in this frequency range, independent of the presence or absence of H bonds.[66,72] Finally, the small increase in S_{G1} with increasing T is expected for librational motions due to increasing thermal motions, whereas amplitudes usually decrease for vibrations. It should be noted here that although ILs containing pyrrolidinium, tetraalkylammonium, and tetraalkylphosphonium cations exhibit a mode at ∼60 cm^{-1} that may be associated with interionic stretching vibrations,[73,74] albeit with librational and cross-contributions, this is unlikely to be the source of the G_1 mode for EAN and PAN because the masses of NO_3^- and $EtNH_3^+$ or, respectively, $PrNH_3^+$, are too small for such a low resonance frequency.

With regard to the G_2' mode in the OKE spectra of EAN, it can be speculated that it is related to cation motions as $S_{G2'} \ll S_{G1}$ (Figure 5a, inset), in line with the respective polarizability anisotropies of NO_3^- and $EtNH_3^+$ (Section 4.2). The frequency maximum of G_2' in the OKE spectra lies between those of the G_2 and G_3 modes in the DR spectra, which suggests that it is a composite mode that can be resolved in the DR but not in the OKE spectra. Furthermore, the slight increase in $S_{G2'}$ with increasing T (Figure 9d) implies that the librational portion (as discussed later) predominates in G_2', consistent with the fact that OKE is mainly sensitive to rotational motions.

dx.doi.org/10.1021/jp502935t | J. Phys. Chem. B 2015, 119, 8826−8841

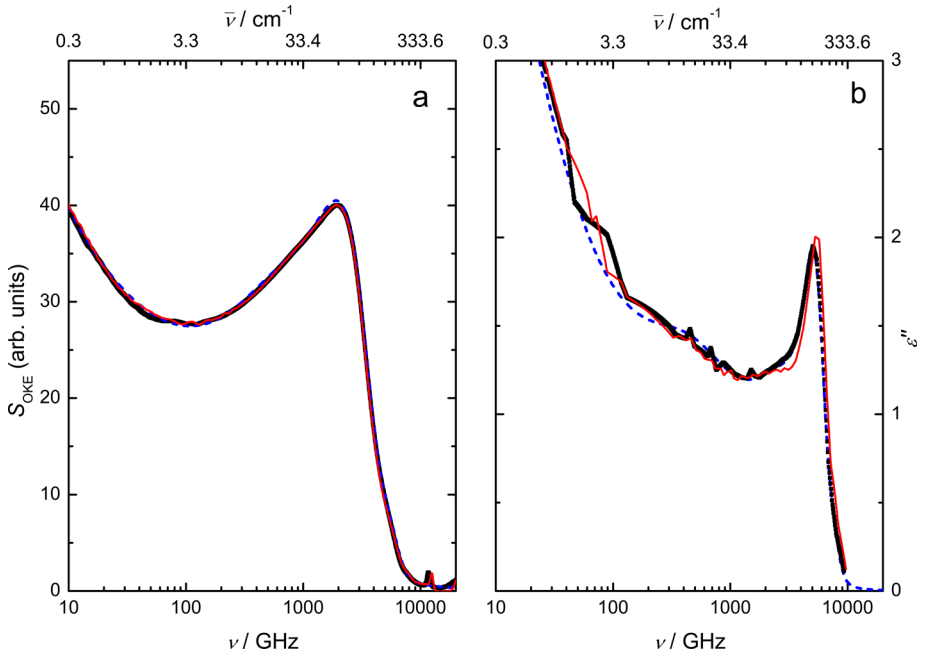

Figure 10. (a) OKE and (b) DR spectra of EAN (red solid lines) and d_3-EAN (■) with the corresponding total fit of d_3-EAN (dashed blue lines) at 25 °C.

DRS Fits. As described in Section 3.2 the high-frequency part of the DR spectra of EAN was fitted by a model consisting of a damped harmonic oscillator, DHO_1 (~1.5 THz), three Gaussians, G_1 (~2.0 THz), G_2 (~4.5 THz), and G_3 (~5.6 THz), plus an additional mode, DHO_2 (7.9 THz), that is associated with the intramolecular torsion of the ethyl group of $EtNH_3^+$ (Table 1).[13]

It is reiterated here (see also Section 3.2) that while this model provided the best fit of the observed DR spectra, it is not the only possible approach. This uncertainty is partially due the strongly overlapping contributions from coupled multiple–particle interactions and also because of significant technical limitations on the accuracy of the spectra, particularly in the low-terahertz range. These problems evidence themselves by a small underestimation of the observed intensities at intermediate frequencies: $50 \lesssim \nu/\mathrm{GHz} \lesssim 1000$ (Figure 5). Nevertheless, as argued in Section 3.2, inclusion of further processes, for example, a constant loss term[18] or an additional Debye function at ~80 GHz, yielded no improvement in the fits. Fortunately, the imperfectly fitted intermediate frequency range is sufficiently well-separated from the high-frequency ($\nu >$ 1 THz) region that is of special interest here because of what it may reveal about the similarities (or otherwise) between EAN and water.[13,67,70]

All fit parameters for the modes in this region of the dielectric spectra of EAN (Figures 9a–c) and PAN (see Section 5.3 below) showed reasonably smooth trends with temperature. Thus, the resonance frequencies decreased slightly with increasing T for all modes (Figure 9c), as for the OKE fits (Figure 9f). But again this trend does not distinguish between librational and vibrational contributions because, as observed for water,[75,76] ν_0 of H-bond stretching also decreases with increasing T. The corresponding DR amplitudes (Figure 9a) differed in their temperature dependence: S_{G1} (▲) and S_{G3} (■) increased with increasing T, whereas S_{DHO_1} (□) and S_{G2} (△) decreased. This must mean, in contrast with the model of Fumino et al.,[13] not all of the present Gaussian modes can be due to intermolecular H-bond vibrations. If so, they would be expected to decrease in amplitude with increasing T due to the weakening of the H bonds.

While G_1 in OKE (Figure 5a) can be confidently assigned to nitrate libration, its relatively weak equivalent in DRS (Figure 5b) may be related to the collision-induced part of this mode. The reasons for this tentative assignment are first because $\nu_{G1}^{DR} \approx \nu_{G1}^{OKE}$ and second because S_{G1}^{DR} increased with T (Figure 9a, ▲). The latter is what would be expected for an interaction-induced contribution (and a libration) because of the increasing collision rate due to increasing thermal motions. For H-bond vibrations, the opposite trend is expected because of the decreasing liquid density and H-bond weakening. A similar situation was found for G_3: because its amplitude increased with increasing T (Figure 9a, ■), it is reasonable to associate it with cation librations.[77]

In contrast with S_{G1} and S_{G3}, the magnitude of S_{G2} decreased with increasing T (Figure 9a, △). Such a trend is compatible with H-bond vibrations, as observed for water.[13,77] If so, G_2 can be attributed to H-bond stretching, which is more energetic than H-bond bending. This means H-bond bending (if such a contribution exists) might be a possible origin of the DHO_1 mode. This assignment of DHO_1 is consistent with that of Fumino et al.[13] and is supported by the drop in S_{DHO_1} with increasing T (Figure 9a, □). It should be noted, however, that DHO_1 may also include a contribution from a possible CL mode.

5.2. Deuterated EAN. The H atoms of the ammonium group of EAN were ~91% replaced by deuterium atoms, corresponding to an average composition of $[EtND_{2.7}H_{0.3}]^+$ which, for convenience, will referred to throughout as d_3-EAN. Because of time and material constraints, DR and OKE spectra of d_3-EAN were recorded only at 25 °C. Both spectra were found to be fitted satisfactorily with the same models used for EAN (Section 3.2).

OKE Spectrum. The OKE spectrum of d_3-EAN is compared with that of EAN in Figure 10a. The two 25 °C spectra match

dx.doi.org/10.1021/jp502935t | J. Phys. Chem. B 2015, 119, 8826–8841

almost perfectly, showing no isotopic shift (IS) and providing nearly identical fit parameters (Table S3 in the Supporting Information). Although the calculated IS for a H-bond vibration (~2%, see below) is at the present detection limit, the close similarity of the OKE spectra of EAN and d_3-EAN (Figure 10a) is compatible with the assignment of G_1 (the dominant mode at ~68 cm^{-1}, 2 THz, Figure 5a) to nitrate libration. However, it must be noted that almost no ISs are observed for H-bond vibrations in water,[70] so the absence of a detectable IS for G_1(EAN, d_3-EAN) is not definitive.

DR Spectrum. The situation is different for the dielectric spectrum. Figure 11 compares the present $\hat{\varepsilon}(\nu)$ data for d_3-EAN and EAN at 25 °C with the FIR results for EAN at 80 °C obtained by Fumino et al.[13] For comparison purposes, the present spectra have been converted to the relative absorption format, $\alpha_{rel}(\overline{\nu})$, after subtraction of S_α from the total intensity.

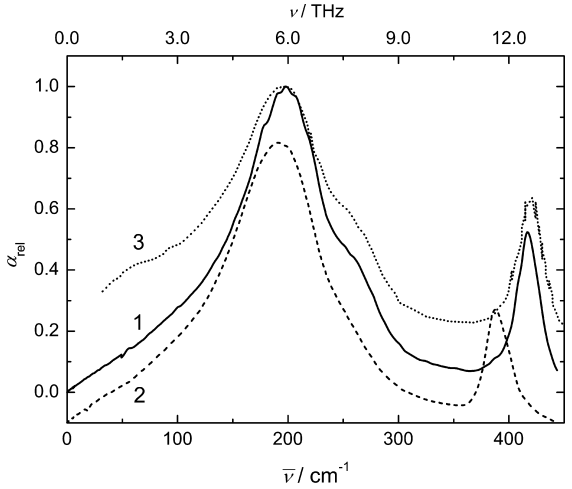

Figure 11. FIR absorption spectra, as $\alpha_{rel}(\overline{\nu})$, of EAN (1, solid line) and d_3-EAN (2, dashed line) at 25 °C (this work) and of EAN at 80 °C (3, dotted line).[13] For visual clarity, a negative offset has been applied to the spectrum of d_3-EAN.

The present EAN spectrum (Figure 11, curve 1) is in qualitative agreement with that of Fumino et al.[13] (Figure 11, curve 3), but, even when allowing for a possible small contribution of S_α to the latter spectrum, it appears that the intensity observed by Fumino et al.[13] is considerably overestimated at $\overline{\nu}$ < 100 cm^{-1}. This is not a criticism of their work but rather a reflection of the difficulty of measurements in this frequency range, which has implications for the fitting of such spectra.

Comparison of curves 1 and 2 in Figure 11 provides information on the EAN/d_3-EAN isotope shifts. A strong IS is observed for the pronounced resonance at ~420 cm^{-1}, associated with the intramolecular bending motion of the cation,[13] which is shifted to ~380 cm^{-1} by deuteration. A smaller but still significant IS is also observed for the peak of $\alpha_{rel}(\overline{\nu})$ at ~200 cm^{-1}, which corresponds to the peak in $\varepsilon''(\nu)$ at ~5.5 THz (Figure 10b). If G_2 is due to H-bond stretching and G_3 to cation librations (as proposed in Section 5.1), the effects of deuteration on these two modes should differ from each other. For H-bond stretching, an IS of $(\mu'_{EAN}/\mu'_{d3EAN})^{1/2}$ = 0.982, where μ' is the reduced mass, would be expected in the gas phase. For cation librations, IS = $(I_{EA+}/I_{d3EA+})^{1/2}$ should be 0.938 or 0.944, depending on the axis of inertia chosen for the cation.[78] The experimental ratios of the resonance frequencies are $\nu_{0,G2}^{d3EAN}/\nu_{0,G2}^{EAN}$ = 0.989 and $\nu_{0,G3}^{d3EAN}/\nu_{0,G3}^{EAN}$ = 0.923. These values differ significantly from each other and, more importantly, are gratifyingly close (given the assumptions involved) to the values of 0.982 predicted for H-bond stretching (G_2) and 0.938/0.944 for cation libration (G_3). These assignments are also consistent with the temperature dependences of S_{G2} and S_{G3} observed for EAN (Figure 9a).

5.3. PAN. The high-frequency region of the DR spectra of PAN was fitted with the same model as that derived for EAN (Section 3.2): a damped harmonic oscillator, DHO_1 (at ~1.6 THz), three Gaussians, G_1 (~2.0 THz), G_2 (~4.8 THz), and G_3 (~6.5 THz), plus an additional mode (DHO_2 at 9.0 THz) associated with the intramolecular torsion of the propyl chain of $PrNH_3^+$ with respect to the $-NH_3^+$ group and which

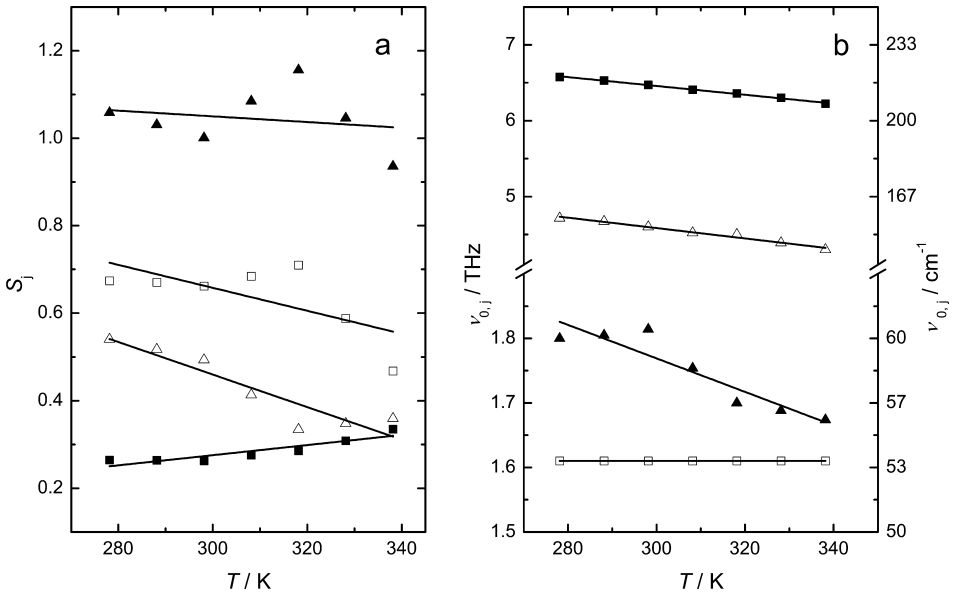

Figure 12. (a) Amplitudes, S_j, and (b) resonance frequencies, $\nu_{0,j}$, of the high-frequency resonance processes DHO_1 (□), G_1 (▲), G_2 (△), and G_3 (■) obtained from the fit of the DR spectra of PAN as a function of temperature. Solid lines are linear regressions of the data.

dx.doi.org/10.1021/jp502935t | J. Phys. Chem. B 2015, 119, 8826−8841

includes the intramolecular bending vibration of the propyl chain.[13,79]

It is not surprising (given their similar chemical structures) but is nevertheless gratifying that the model used to describe the DR spectra of EAN should also be applicable to PAN because it provides circumstantial evidence of the reasonableness of the EAN model. For example, the somewhat ad hoc introduction (Section 5.1) of an additional Gaussian (G_3) centered at ∼6 GHz to best describe the DR spectrum of EAN at high frequencies is supported by the clear-cut presence of a shoulder at ∼7 THz in the DR spectrum of PAN in addition to the pronounced peak at ∼5 THz described by G_2, compare Figures 4 and 6. This provides strong support for more than one mode being responsible for the observed intensity in this region, consistent with the published FIR spectra.[13,79]

The amplitudes of the DHO_1, G_1, G_2, and G_3 modes for PAN are plotted in Figure 12a. For all S_j, the effect of T was the same as for EAN,[80] again supporting the present mode assignments. Thus, the resonance frequencies $\nu_{0,G1}$, $\nu_{0,G2}$, and $\nu_{0,G3}$ of PAN decreased with increasing T (Figure 12b), as observed for EAN (Figure 9c) with the partial exception of $\nu_{0,G1}$. It is observed that $\nu_{0,G3}$ differs significantly (by ∼0.8 THz) between PAN and EAN, whereas $\nu_{0,G2}$ is almost the same (compare Figures 9c and 12b). Again such a difference is consistent with the assignment of G_2 and G_3 to different molecular-level processes.[81]

To summarize, the present model provides a consistent description of the fast dynamics of EAN, d_3-EAN, and PAN. In particular, it shows that the observed DR and OKE intensities at high frequencies ($\overline{\nu} \gtrsim 50$ cm^{-1}) cannot be due to H-bond vibrations alone, as has been proposed on the basis of FIR measurements and DFT calculations.[13,79] Rather, there are also significant additional contributions from anion and cation librations (the G_1 and G_3 modes).

5.4. Intermediate Frequency Range. Sophisticated MD simulations and more accurate experimental studies will be required to fully understand the dynamics of PILs in the intermediate frequency range ($0.05 \lesssim \nu/\mathrm{THz} \lesssim 1$) given the probable complexity of the contributing modes. The present DR and OKE spectra of EAN and PAN, like those observed for other ILs,[17,82] show a finite but featureless intensity over this range. This intensity reflects the strong coupling or overlap of the potentially numerous rotational and translational modes that are expected to occur in this region. Thus, the spectral contributions from the motions of individual molecular-level species, the oscillation of the cages formed by the surrounding neighbors, and the decay of these cages blur into a continuous distribution of states. For PILs such as EAN and PAN, fast proton transfers may also occur on this time scale. The combination of these factors makes a definitive separation and identification of the contributing processes a futile exercise at the present time. Accordingly, as already mentioned, the intensity of the OKE spectrum of EAN at intermediate frequencies was described by a constant-loss term of amplitude, S_{CL}, which substitutes for all possible contributions in this region. In contrast, in the DR spectrum of EAN and PAN, where this intensity is considerably smaller, it was more appropriate to subsume it in the CDi (α relaxation) and DHO_1 modes.

For supercooled liquids, contributions on this time scale have been referred to as β-relaxations.[83] Although the specific contributions to the β-relaxation are unknown, it seems likely that they originate, at least in part, from the motions of mobile clusters in an almost frozen environment, as proposed for glass-forming systems.[83,84] Such motions are notionally comparable with the "cage rattling" translational motions suggested for imidazolium-based ILs in the same spectral region.[53]

An additional contribution in this intermediate region might be analogous to the "frame tumbling" proposed for water.[60] In contrast with librations, this motion involves H-bond exchange and can be seen as a preliminary (faster) stage of the H-bond making and breaking associated with the α-relaxation. Support for the presence of such a process in EAN comes from an MD simulation of the closely related methylammonium nitrate (MAN).[85] This simulation predicts that H-bond making and breaking takes place within ∼0.5 ps, while proton hopping happens within ∼3 ps. Both processes are potential candidates for the observed intensity in the intermediate frequency range.

6. CONCLUSIONS

The present combination of broadband DR and OKE spectroscopies, covering the exceptionally wide frequency range of $0.2 \lesssim \nu/\mathrm{GHz} \lesssim 10000$ and (for most measurements) a temperature range of $5 \leq \vartheta/°\mathrm{C} \leq 65$, has provided detailed insights into the dynamics of the archetypal PIL EAN and its congener PAN.

At lower frequencies ($\nu \lesssim 100$ GHz), the α-relaxation for EAN and PAN in the DR and OKE spectra could reasonably be assigned to the reorientation of the cations and the anions, respectively. A high degree of cooperativity in these motions was evident from the observed departures of the relaxation times from SED behavior and the similarities of the activation energies, E_A^{OKE} and E_A^{DR}. This is consistent with the presence of strong and directed interionic interactions associated with strong H bonding between the anions and cations, in line with previous studies of EAN mixtures with acetonitrile.[86] Moreover, comparison of τ_α^{DR} for EAN with data from fs-IR spectroscopy[57] indicates that the relaxation mechanism of the ions is not diffusive but instead occurs through large-angle jump reorientations, with the jump angle being consistent with the pseudotetrahedral geometry of the alkylammonium ion. This suggests that in addition to the expected Coulombic interactions, multiple H-bonding between $EtNH_3^+$ and NO_3^- plays an important role in determining the MD of EAN. The unusual negative temperature dependence of μ_{eff} for EAN and PAN, also supports the picture of PIL relaxations as being highly cooperative.

While the exact origins of the featureless intensity in the intermediate frequency region ($0.05 \lesssim \nu/\mathrm{THz} \lesssim 1$) remain unclear, detailed insights into the high-frequency dynamics could still be obtained. Analysis of the DR and OKE spectra of EAN, supplemented by the DR spectra of PAN, as a function of temperature and OKE and DR spectra of d_3-EAN at 25 °C, indicated that in the frequency range $1 \lesssim \nu/\mathrm{THz} \lesssim 10$, intermolecular (i.e., interionic) H-bond vibrations (bending and stretching) overlap with anion and cation librations. The present assignments of the high-frequency modes (Table 1) confirm in part those of some of the features in the FIR spectra identified by Fumino et al.[13] but also show that ion librations, ignored by Fumino et al., contribute significantly to the observed spectra. The present assignments are broadly supported by the isotopic shifts observed in the FIR spectra of EAN and d_3-EAN.

While much has been learnt from the present investigation, further experimental studies using improved equipment and more sophisticated MD simulations that quantitatively

dx.doi.org/10.1021/jp502935t | J. Phys. Chem. B 2015, 119, 8826−8841

reproduce the DR and OKE spectra will be required for a fuller understanding of the dynamics of typical PILs such as EAN.

■ ASSOCIATED CONTENT

Supporting Information

Tables with physicochemical properties and relaxation parameters. This material is available free of charge via the Internet at http://pubs.acs.org.

■ AUTHOR INFORMATION

Corresponding Author

*E-mail: Richard.Buchner@chemie.uni-regensburg.de.

Notes

The authors declare no competing financial interest.

■ ACKNOWLEDGMENTS

We thank Prof. W. Kunz (Universität Regensburg) for the provision of laboratory facilities and the Deutsche Forschungsgemeinschaft for funding within the Priority Program 1191.

■ REFERENCES

(1) Greaves, T. L.; Drummond, C. J. Protic Ionic Liquids: Properties and Applications. *Chem. Rev.* **2008**, *108*, 206−237.

(2) Evans, D. F.; Chen, S.-H. Thermodynamics of Solution of Nonpolar Gases in a Fused Salt. "Hydrophobic Bonding" in a Nonaqueous System. *J. Am. Chem. Soc.* **1981**, *103*, 481−482.

(3) Earle, M. J.; Esperanca, J. M. S. S.; Gilea, M. A.; Lopes, J. N. C; Rebelo, L. P. N.; Magee, J. W.; Seddon, K. R.; Widegren, J. A. The Distillation and Volatility of Ionic Liquids. *Nature* **2006**, *439*, 831−834.

(4) MacFarlane, D. R.; Pringle, J. M.; Johansson, K. M.; Forsyth, S.; Forsyth, M. Lewis Base Ionic Liquids. *Chem. Commun.* **2006**, 1905−1917.

(5) Susan, M. A. B. H.; Noda, A.; Mitsushima, S.; Watanabe, M. Brønsted Acid-base Ionic Liquids and their Use as New Materials for Anhydrous Proton Conductors. *Chem. Commun.* **2003**, 938−939.

(6) Rana, U. A.; Forsyth, M.; MacFarlane, D. R.; Pringle, J. M. Toward Protic Ionic Liquid and Organic Plastic Crystal Electrolytes for Fuel Cells. *Electrochim. Acta* **2012**, *84*, 213−222.

(7) Walden, P. Molecular Weights and Electrical Conductivities of Several Fused Salts. *Bull. Russ. Acad. Sci.* **1914**, *8*, 405−422.

(8) Zech, O.; Thomaier, S.; Kolodziejski, A.; Touraud, D.; Grillo, I.; Kunz, W. Ethylammonium Nitrate in High Temperature Stable Microemulsions. *J. Colloid Interface Sci.* **2010**, *347*, 227−232.

(9) Hayes, R.; Imberti, S.; Warr, G.; Atkin, R. Amphiphilicity Determines Nanostructure in Protic Ionic Liquids. *Phys. Chem. Chem. Phys.* **2011**, *13*, 3237−3247.

(10) Gontrani, L.; Bodo, E.; Triolo, A.; Leonelli, F.; D'Angelo, P.; Migliorati, V.; Caminiti, R. The Interpretation of Diffraction Patterns of Two Prototypical Protic Ionic Liquids: a Challenging Task for Classical Molecular Dynamics Simulations. *J. Phys. Chem. B* **2012**, *116*, 13024−13032.

(11) Umebayashi, Y.; Chung, W.; Mitsugi, T.; Fukuda, S.; Takeuchi, M.; Fujii, K.; Taka-muku, T.; Kanzaki, R.; Ishiguro, S. Liquid Structure and the Ion-Ion Interactions of Ethylammonium Nitrate Ionic Liquid Studied by Large-Angle X-Ray Scattering and Molecular Dynamics Simulations. *J. Comput. Chem. Jpn.* **2008**, *7*, 125−134.

(12) Song, X.; Hamano, H.; Minofar, B.; Kanzaki, R.; Fujii, K.; Kameda, Y.; Kohara, S.; Watanabe, M.; Ishiguro, S.; Umebayashi, Y. Structural Heterogeneity and Unique Distorted Hydrogen Bonding in Primary Ammonium Nitrate Ionic Liquids Studied by High-Energy X-ray Diffraction Experiments and MD Simulation. *J. Phys. Chem. B* **2012**, *116*, 2801−2813.

(13) Fumino, K.; Wulf, A.; Ludwig, R. Hydrogen Bonding in Protic Ionic Liquids: Reminiscent of Water. *Angew. Chem., Int. Ed.* **2009**, *48*, 5184−5186.

(14) Fumino, K.; Reichert, E.; Wittier, K.; Hempelmann, R.; Ludwig, R. Low-Frequency Vibrational Modes of Protic Molten Salts and Ionic Liquids: Detecting and Quantifying Hydrogen Bonds. *Angew. Chem., Int. Ed.* **2012**, *51*, 6236−6240.

(15) Weingärtner, H.; Knocks, A.; Schrader, W.; Kaatze, U. Dielectric Spectroscopy of the Room Temperature Molten Salt Ethylammonium Nitrate. *J. Phys. Chem. A* **2001**, *105*, 8646−8650.

(16) Krüger, M.; Bründermann, E.; Funkner, S.; Weingärtner, H.; Havenith, M. Polarity Fluctuations of the Protic Ionic Liquid Ethylammonium Nitrate in the Terahertz Regime. *J. Chem. Phys.* **2010**, *132*, 101101.

(17) Turton, D. A.; Hunger, J.; Stoppa, A.; Hefter, G.; Thoman, A.; Walther, M.; Buchner, R.; Wynne, K. Dynamics of Imidazolium Ionic Liquids from a Combined Dielectric Relaxation and Optical Kerr Effect Study: Evidence for Mesoscopic Aggregation. *J. Am. Chem. Soc.* **2009**, *131*, 11140−11146.

(18) Turton, D. A.; Sonnleitner, T.; Ortner, A.; Walther, M.; Hefter, G.; Seddon, K. R.; Stana, S.; Plechkova, N.; Buchner, R.; Wynne, K. Structure and Dynamics in Protic Ionic Liquids: A Combined Optical Kerr-effect and Dielectric Relaxation Spectroscopy Study. *Faraday Discuss.* **2012**, *154*, 145−153.

(19) Sonnleitner, T.; Turton, D.; Waselikowski, S.; Hunger, J.; Stoppa, A.; Walther, M.; Wynne, K.; Buchner, R. Dynamics of RTILs: A Comparative Dielectric and OKE Study. *J. Mol. Liq.* **2014**, *192*, 19−25.

(20) Evans, D. F.; Yamauchi, A.; Roman, R.; Casassa, E. Z. Micelle Formation in Ethylammonium Nitrate, a Low-Melting Fused Salt. *J. Colloid Interface Sci.* **1982**, *88*, 89−96.

(21) Kremer, F.; Schönhals, A. *Broadband Dielectric Spectroscopy*; Springer, Berlin, 2003.

(22) Buchner, R.; Hefter, G. Interactions and Dynamics in Electrolyte Solutions by Dielectric Spectroscopy. *Phys. Chem. Chem. Phys.* **2009**, *11*, 8984−8999.

(23) Barthel, J.; Buchner, R.; Eberspächer, P. N.; Münsterer, M.; Stauber, J.; Wurm, B. Dielectric Relaxation in Electrolyte Solutions. Recent Developments and Prospects. *J. Mol. Liq.* **1998**, *78*, 83−109.

(24) Schrödle, S.; Hefter, G.; Kunz, W.; Buchner, R. Effects of Nonionic Surfactant $C_{12}E_5$ on the Cooperative Dynamics of Water. *Langmuir* **2006**, *22*, 924−932.

(25) Jepsen, P.; Fischer, B. M.; Thoman, A.; Helm, H.; Suh, J. Y.; Lopez, R.; Haglund, R. F. Metal-insulator phase Transition in a VO_2 Thin Film Observed with Terahertz Spectroscopy. *Phys. Rev. B* **2006**, *74*, 205103.

(26) Hunger, J.; Stoppa, A.; Thoman, A.; Walther, M.; Buchner, R. Broadband Dielectric Response of Dichloromethane. *Chem. Phys. Lett.* **2009**, *471*, 85−91.

(27) Böttcher, C. F. J. *Theory of Electric Polarization*; Elsevier: Amsterdam, 1973; Vol. *1*.

(28) Böttcher, C. F. J.; Bordewijk, P. *Theory of Electric Polarization*; Elsevier: Amsterdam, 1978; Vol. *2*.

(29) Fecko, C. J.; Eaves, J. D.; Tomakoff, A. Isotropic and Anisotropic Raman Scattering from Molecular Liquids Measured by Spatially Masked Optical Kerr Effect Spectroscopy. *J. Chem. Phys.* **2002**, *117*, 1139−1154.

(30) Shaukat, S.; Buchner, R. Densities, Viscosities [from (278.15 to 318.15) K], and Electrical Conductivities (at 298.15 K) of Aqueous Solutions of Choline Chloride and Chloro-Choline Chloride. *J. Chem. Eng. Data* **2011**, *56*, 4944−4949.

(31) Greaves, T. L.; Weerawardena, A.; Fong, C.; Krodkiewska, I.; Drummond, C. J. Protic Ionic Liquids: Solvents with Tunable Phase Behavior and Physicochemical Properties. *J. Phys. Chem. B* **2006**, *110*, 22479−22487.

(32) Poole, C. F.; Kersten, B. R.; Ho, S. S.; Coddens, M. E.; Furton, K. G. Organic Salts, Liquid at Room Temperature, as Mobile Phases in Liquid Chromatography. *J. Chromatogr.* **1986**, *352*, 407−425.

(33) Shetty, P. H.; Youngberg, P. J.; Kersten, B. R.; Poole, C. F. Solvent Properties of Liquid Organic Salts used as Mobile Phases in Microcolumn Reversed-Phase Liquid Chromatography. *J. Chromatogr.* **1987**, *411*, 61−79.

(34) Atkin, R.; Warr, G. The smallest Amphiphiles: Nanostructure in Protic Room-Temperature Ionic Liquids with Short Alkyl Groups. *J. Phys. Chem. B* **2008**, *112*, 4146−4166.
(35) Belieres, J.-P.; Angell, C. A. Protic Ionic Liquids: Preparation, Characterization, and Proton Free Energy Level Representation. *J. Phys. Chem. B* **2007**, *111*, 4926−4937.
(36) Oleinikova, A.; Bonetti, M. Critical Behavior of the Electrical Conductivity of Concentrated Electrolytes: Ethylammonium Nitrate in n-Octanol Binary Mixtures. *J. Solution Chem.* **2002**, *31*, 397−413.
(37) Ferry, J. D. *Viscoelastic Properties of Polymers*; Wiley: New York, 1980.
(38) Angell, C. A. Relaxation in Liquids, Polymers and Plastic Crystals—Strong/Fragile Patterns and Problems. *J. Non-Cryst. Solids* **1991**, *131*−*133*, 13−31.
(39) Smith, J. A.; Webber, G. B.; Warr, G. G.; Atkin, R. Rheology of Protic Ionic Liquids and Their Mixtures. *J. Phys. Chem. B* **2013**, *117*, 13930−13935.
(40) Bouzón Capelo, S.; Méndez-Morales, T.; Carrete, J.; López Lago, E.; Vila, J.; Cabeza, O.; Rodriguez, J. R.; Turmine, M.; Varela, L. M. Effect of Temperature and Cationic Chain Length on the Physical Properties of Ammonium Nitrate-Based Protic Ionic Liquids. *J. Phys. Chem. B* **2012**, *116*, 11302−11312.
(41) Schröder, C.; Steinhauser, O. In *Computational Dielectric Spectroscopy of Charged, Dipolar Systems*; Grünenberg, J., Ed.; Wiley-VCH: Weinheim, Germany, 2010.
(42) Schröder, C.; Haberler, M.; Steinhauser, O. On the Computation and Contribution of Conductivity in Molecular Ionic Liquids. *J. Chem. Phys.* **2008**, *128*, 134501.
(43) Schröder, C. Collective Translational Motions and Cage Relaxations in Molecular Ionic Liquids. *J. Chem. Phys.* **2011**, *135*, 024502.
(44) Ishida, T.; Nishikawa, K.; Shirota, H. Atom Substitution Effects of $[XF_6]^-$ in Ionic Liquids. 2. Theoretical Study. *J. Phys. Chem. B* **2009**, *113*, 9840−9851.
(45) Ishida, T.; Shirota, H. Dicationic versus Monocationic Ionic Liquids: Distinctive Ionic Dynamics and Dynamical Heterogeneity. *J. Phys. Chem. B* **2009**, *117*, 1136−1150.
(46) Schröder, C.; Sonnleitner, T.; Buchner, R.; Steinhauser, O. The Influence of Polarizability on the Dielectric Spectrum of the Ionic Liquid l-Ethyl-3-imidazolium Triflate. *Phys. Chem. Chem. Phys.* **2011**, *13*, 12240−12248.
(47) Turton, D.; Wynne, K. Structural Relaxation in the Hydrogen-bonding Liquids N-methylacetamide and Water Studied by Optical Kerr Effect Spectroscopy. *J. Chem. Phys.* **2008**, *128*, 154516.
(48) Chalmers, J. M.; Griffiths, P. R. *Handbook of Vibrational Spectroscopy*; Wiley-VCH: Weinheim, Germany, 2001.
(49) *NIST Handbook of Mathematical Functions*; Lozier, D. M., Boisvert, R. F., Clark, C. W., Eds.; Cambridge Univ. Press: Cambridge, U.K., 2010.
(50) Hunger, J.; Stoppa, A.; Schrödle, S.; Hefter, G.; Buchner, R. Temperature Dependence of the Dielectric Properties and Dynamics of Ionic Liquids. *ChemPhysChem* **2009**, *10*, 723−733.
(51) Cang, H.; Novikov, N.; Fayer, M. D. Logarithmic Decay of the Orientational Correlation Function in Supercooled Liquids on the ps to ns Time Scale. *J. Chem. Phys.* **2003**, *118*, 2800−2807.
(52) Buchner, R.; Chen, T.; Hefter, G. Complexity in Simple Electrolyte Solutions: Ion Pairing in $MgSO_4$(aq). *J. Phys. Chem. B* **2004**, *108*, 2365−2375.
(53) Turton, D.; Corsaro, C.; Candelaresi, M.; Brownlie, A.; Seddon, K. R.; Mallamace, F.; Wynne, K. The Structure and Terahertz Dynamics of Water Confined in Nanoscale Pools in Salt Solutions. *Faraday Discuss.* **2011**, *150*, 493−504.
(54) Huang, M.-M.; Jiang, Y.; Sasisanker, P.; Driver, G. W.; Weingärtner, H. Static Relative Dielectric Permittivities of Ionic Liquids at 25°C. *J. Chem. Eng. Data* **2011**, *56*, 1494−1499.
(55) Salvador, P.; Curtis, J. E.; Tobias, D. J.; Jungwirth, P. Polarizability of the Nitrate Anion and its Solvation at the Air/Water Interface. *Phys. Chem. Chem. Phys.* **2003**, *5*, 3752−3757.
(56) Stewart, J. J. P. M. *MOPAC*; Stewart Computational Chemistry: Colorado Springs, CO, USA, 2009.
(57) Hunger, J.; Sonnleitner, T.; Liu, L.; Buchner, R.; Bonn, M.; Bakker, H. J. Hydrogen-Bond Dynamics in a Protic Ionic Liquid: Evidence of Large-Angle Jumps. *J. Phys. Chem. Lett.* **2012**, *3*, 3034−3038.
(58) Note that for comparison with the fs-IR relaxation times, the Cole−Davidson relaxation times, τ_α^{DR}, obtained from the dielectric fit were converted into relaxation times of the α-peak maximum, $\tau_{\alpha,max}^{DR}$, using equation 4 in ref 87.
(59) Shim, Y.; Kim, H. Dielectric Relaxation, Ion Conductivity, Solvent Rotation, and Sol-vation Dynamics in Room-Temperature Ionic Liquid. *J. Phys. Chem. B* **2008**, *112*, 11028−11038.
(60) Laage, D.; Stirnemann, G.; Sterpone, F.; Rey, R.; Hynes, J. T. Reorientation and Allied Dynamics in Water and Aqueous Solutions. *Annu. Rev. Phys. Chem.* **2011**, *62*, 395−416.
(61) Ohmine, I.; Tanaka, H. Fluctuation, Relaxations, and Hydration in Liquid Water. Hydrogen-Bond Rearrangement Dynamics. *Chem. Rev.* **1993**, *93*, 2545−2566.
(62) Izgorodina, E. I.; Forsyth, M.; MacFarlane, D. R. On the Components of the Dielectric Constants of Ionic Liquids: Ionic Polarization? *Phys. Chem. Chem. Phys.* **2009**, *11*, 2452−2458.
(63) Barthel, J.; Hetzenauer, H.; Buchner, R. Dielectric Relaxation of Aqueous Electrolyte Solutions. II. Ion-Pair Relaxation of 1:2, 2:1, and 2:2 Electrolytes. *Bunsen-Ges. Phys. Chem., Ber.* **1992**, *96*, 1424−1432.
(64) Scholte, T. A Contribution to the Theory of the Dielectric Constant of Polar Liquids. *Physica* **1949**, *15*, 437−449.
(65) The difference between μ_{eff} and μ_{app} of PAN can be explained by the fact that in the liquid phase the pivot does not necessarily coincide with the center of gravity but more likely with the center of hydrodynamic stress;[63] the higher flexibility of $PrNH_3^+$ may also play a role.
(66) Heisler, I. A.; Meech, S. R. Polarization-Resolved Ultrafast Polarizability Relaxation in Polar Aromatic Liquids. *J. Phys. Chem. B* **2008**, *112*, 12976−12984.
(67) Fukasawa, T.; Sato, T.; Watanabe, J.; Hama, Y.; Kunz, W.; Buchner, R. Relation between Dielectric and Low-Frequency Raman Spectra of Hydrogen-Bond Liquids. *Phys. Rev. Lett.* **2005**, *95*, 197802.
(68) Winkler, K.; Lindner, J.; Vöhringer, P. Low-frequency Depolarized Raman-Spectral Density of Liquid Water from Femtosecond Optical Kerr-Effect Measurements: Line-shape Analysis of Restricted Translational Modes. *Phys. Chem. Chem. Phys.* **2002**, *4*, 2144−2155.
(69) Bartoli, F. J.; Litovitz, T. A. Raman Scattering: Orientational Motions in Liquids. *J. Chem. Phys.* **1972**, *56*, 413−425.
(70) Zelsmann, H. R. Temperature Dependence of the Optical Constants for Liquid H_2O and D_2O in the Far IR Region. *J. Mol. Struct.* **1995**, *350*, 95−114.
(71) Castner, E. W.; Maroncelli, M. Solvent Dynamics Derived from Optical Kerr Effect, Dielectric Dispersion, and Time-Resolved Stokes Shift Measurements: An Empirical Comparison. *J. Mol. Liq.* **1998**, *77*, 1−36.
(72) Palombo, F.; Paolantoni, M.; Sassi, P.; Morresi, A.; Giorgini, M. G. Molecular Dynamics of Liquid Acetone Determined by Depolarized Rayleigh and Low-frequency Raman Scattering Spectroscopy. *Phys. Chem. Chem. Phys.* **2011**, *13*, 16197−16207.
(73) Shirota, H.; Funston, A. M.; Wishart, J. F.; Castner, E. W. Ultrafast Dynamics of Pyrrolidinium Cation Ionic Liquids. *J. Chem. Phys.* **2005**, *122*, 184512.
(74) Shirota, H.; Fukazawa, H.; Fujisawa, T.; Wishart, J. F. Heavy Atom Substitution Effects in Non-Aromatic Ionic Liquids: Ultrafast Dynamics and Physical Properties. *J. Phys. Chem. B* **2010**, *114*, 9400−9412.
(75) Amo, Y.; Tominaga, Y. Low-Frequency Raman Study of Water Isotopes. *Physica A* **2000**, *276*, 401−412.
(76) Gaiduk, V. I.; Nielsen, O. F.; Crothers, D. S. F. Molecular Theory of Low-frequency Raman Spectrum of Water in the Translational-band Region. *J. Mol. Liq.* **2008**, *137*, 92−103.

(77) Brubach, J.-B.; Mermet, A.; Filabozzi, A.; Gerschel, A.; Roy, P. Signatures of the Hydrogen Bonding in the Infrared Bands of Water. *J. Chem. Phys.* **2005**, *122*, 184509.
(78) The relevant moments of inertia determined by MOPAC[56] for EAN and d_3-EAN (assuming rigid molecules) are $I_B = 100.6035 \times 10^{-47}$ kg m^2 and $I_C = 114.4250 \times 10^{-47}$ kg m^2 and $I_B = 114.3995 \times 10^{-47}$ kg m^2 and $I_C = 128.43\ 74 \times 10^{-47}$ kg m^2, respectively. Indices "B" and "C" denote the principle axes of inertia perpendicular to the dipole vector.
(79) Fumino, K.; Wulf, A.; Ludwig, R. The Potential Role of Hydrogen Bonding in Aprotic and Protic Ionic Liquids. *Phys. Chem. Chem. Phys.* **2009**, *11*, 8790−8794.
(80) Except perhaps S_{G1}, which increases with increasing T for EAN (Figure 9a, ▲) but is almost constant for PAN (Figure 12a, ▲). However, this difference may result from the considerable scatter in the THz-TDS data (Figure 4) and the absence of OKE data to fix $\nu_{0,G1}$.
(81) Note, however, that the harmonic oscillator model would predict $\nu_{0,G3}$(EAN) > $\nu_{0,G3}$(PAN), opposite to the present results. This possibly reflects the effects of the greater length (size) and flexibility of the propyl chain on the librational cage. In contrast, G_2 assigned to H-bond stretching would be expected to be less affected when Et is replaced by Pr, because of its translational character.
(82) Stoppa, A.; Hunger, J.; Buchner, R.; Hefter, G.; Thoman, A.; Helm, H. Interactions and Dynamics in Ionic Liquids. *J. Phys. Chem. B* **2008**, *112*, 4854−4858.
(83) Götze, W.; Sjogren, L. Relaxation Processes in Supercooled Liquids. *Rep. Prog. Phys.* **1992**, *55*, 241−376.
(84) Johari, G. P.; Whalley, E. Dielectric Properties of Glycerol in the Range 0.1−105 Hz, 218−357 K, 0−53 kb. *Faraday Symp. Chem. Soc.* **1972**, *6*, 23−42.
(85) Zahn, S.; Thar, J.; Kirchner, B. Structure and Dynamics of the Protic Ionic Liquid Monomethylammonium Nitrate ([CH_3NH_3]-[$N0_3$]) from Ab Initio Molecular Dynamics Simulations. *J. Chem. Phys.* **2010**, *132*, 124506.
(86) Sonnleitner, T.; Nikitina, V.; Nazet, A.; Buchner, R. Do H-Bonds Explain Strong Ion Aggregation in Ethylammonium Nitrate + Acetonitrile Mixtures? *Phys. Chem. Chem. Phys.* **2013**, *15*, 18445−18452.
(87) Diaz-Calleja, R. Comment on the Maximum in the Loss Permittivity for the Havriliak-Negami Equation. *Macromolecules* **2000**, *33*, 8924.